Journal of Sound and Vibration xxx (2018) 1–34

Contents lists available at ScienceDirect

Journal of Sound and Vibration

journal homepage: www.elsevier.com/locate/jsvi

Aeroacoustics research in Europe: The CEAS-ASC report on 2016 highlights

Alexander G. Wilson

Institute of Sound and Vibration Research, University of Southampton, University Road, Southampton SO17 1BJ, UK

ARTICLE INFO

Article history:
Received 22 September 2017
Received in revised form 5 October 2017
Accepted 9 October 2017
Available online xxx

Keywords:
Aeroacoustics
Noise
Numerical modeling

ABSTRACT

The Council of European Aerospace Societies (CEAS) Aeroacoustics Specialists Committee (ASC) supports and promotes the interests of the scientific and industrial aeroacoustics community on the European scale, and European aeronautics activities internationally. Each year, the committee highlights several of the research and development projects in Europe. This paper is the 2016 issue of this collection of Aeroacoustic Highlights, compiled from contributions submitted to the CEAS-ASC.

The contributions are classified under three main headings; Aircraft and Turbomachinery Noise, Experimental and Numerical Methods and Further Applications of Aeroacoustics. A concise summary of the CEAS-ASC workshop held in Southampton, England, in September 2016 is also included in this report.

1. Introduction

The CEAS-ASC each year provides a report summarizing significant advances in aeroacoustic research fields. The present paper corresponds to the 2016 edition of this report. As for previous editions, it would be impossible to give a detailed view of the scientific activity in each research topic, and the present paper focuses on innovative advances and findings from accomplished projects funded by European, industrial or national programmes. The paper is organized as a collection of contributions, divided into sections corresponding to the main topics of research in 2016.

2. CEAS-ASC workshop

The 20th workshop of the Aeroacoustics Specialists Committee of the CEAS was held at the University of Southampton on the 7th and 8th of September 2016. The focus this year was on measurement techniques and analysis methods for aircraft noise. Twenty five papers were presented over the two day period in the five sessions: Source localisation methods 1, Measurement methods for liner characterization, Signal processing methods for fan noise characterisation, Source localisation methods II and Jet noise/combustion noise/flow instabilities. Two key note talks were included. The first was 'The Similarity between Mode Detection and Beamforming' by Dr Pieter Sijtsma of PSA3 and the second on day 2, 'The Advanced Noise Control Fan' by Dr Daniel Sutliff of NASA. A notable inclusion in this year's workshop was the paper from Dr Kevin Britchford of Rolls-Royce plc who gave an industry perspective into the use of measurement techniques for source and mode detection in aero-engines.

https://doi.org/10.1016/j.jsv.2017.10.016

Please cite this article in press as: A.G. Wilson, Aeroacoustics research in Europe: The CEAS-ASC report on 2016 highlights, Journal of Sound and Vibration (2018), https://doi.org/10.1016/j.jsv.2017.10.016

Speakers came from France, Germany, Israel, The Netherlands, Sweden, US, Romania, Russia, and the UK. A total of 42 participants took part in the workshop with members from the UK, France and Germany being most represented.

The workshop highlighted the great advances in measurement techniques, principally through the use of very large microphone arrays made possible through the development of relatively inexpensive data acquisition systems with large numbers of channels. These large arrays now make possible the detection of many hundreds of modes and provide source maps with high spatial resolution. Such methods were applied to flyover noise, testing in wind tunnels, mode detection in scale-model fan rigs and a technique for determining transmission losses across turbomachinery stages. Equally useful, however, were the papers relating to measurement techniques that required comparatively few sensors but which utilised bespoke algorithms. Examples of such methods included the characterisation of liner impedance in grazing flows, a two-microphone technique for broadband mode detection, an in-duct to far-field extrapolation method, and the use of an efficient inverse method for source location that exploits the axi-symmetry of the source distribution in an engine duct.

The numbers of people attending the workshop, and the diversity of papers, confirmed the sustained interest around Europe in the use of source location methods in aeroacoustics.

Submitted by P. Joseph (pfj@isvr.soton.ac.uk)*, Technical Chair CEAS-ASC Workshop 2016, Institute of Sound and Vibration Research, University of Southampton.*

3. Aircraft and Turbomachinery Noise

3.1. Whole aircraft noise and installation effects

3.1.1. Aeroacoustic simulation of a complete H145 helicopter in descent flight

Impulsive blade vortex interactions (BVI) are dominant noise sources during a helicopter's landing approach. So far, limited computational resources and low fidelity numerical methods have prevented prediction at high accuracy. Recent progress by the implementation of a 5th order spatial WENO method and scalability improvements towards massively parallel simulations has allowed for the first time a simulation of an entire helicopter with sufficient accuracy to gain extensive insight into noise generation and emission [1]. The target of the simulation is a landing approach according to ICAO noise certification procedures.

The aerodynamic simulation is carried out with an URANS simulation accurately resolving the impulsive noise of the BVI events using the CFD solver FLOWer. Due to a subordinate contribution of broad-band noise in this flight state, no DES is performed. Flight mechanics and blade elasticity are considered using CAMRAD II. The noise emission is transported to far-

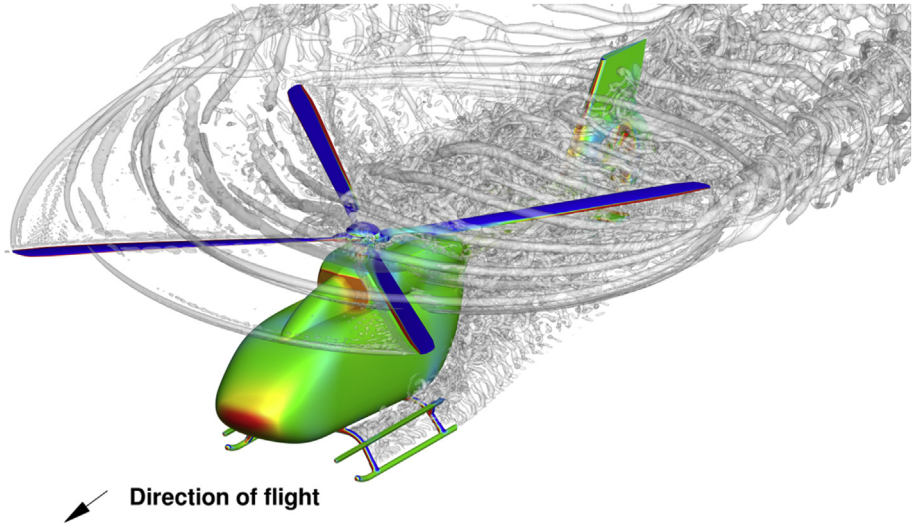

Fig. 1. Vortex visualization (lambda_2 criterion) of the flow field around the H145 in a BVI relevant descent flight with pressure contours on the surface.

Please cite this article in press as: A.G. Wilson, Aeroacoustics research in Europe: The CEAS-ASC report on 2016 highlights, Journal of Sound and Vibration (2018), https://doi.org/10.1016/j.jsv.2017.10.016

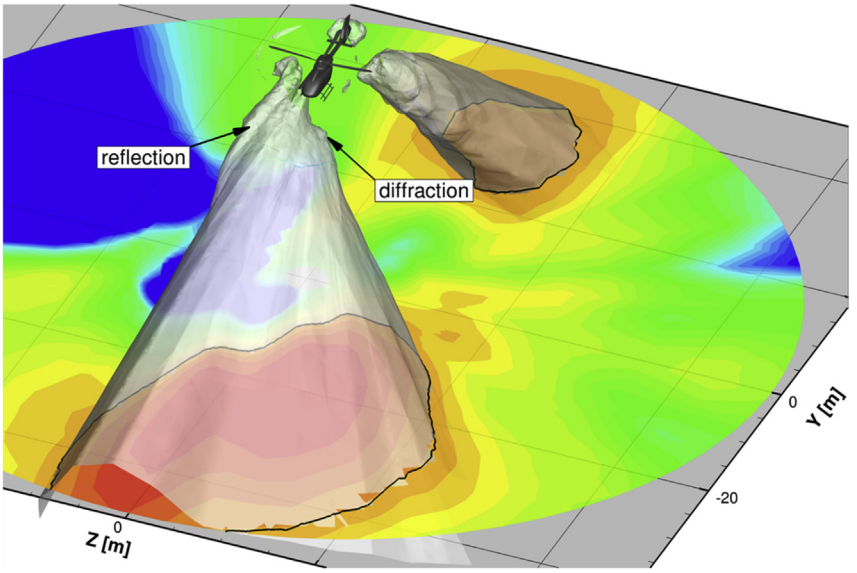

Fig. 2. Radiation of BVI assignable noise emission of the helicopter at 4.5 rotor radii below the helicopter.

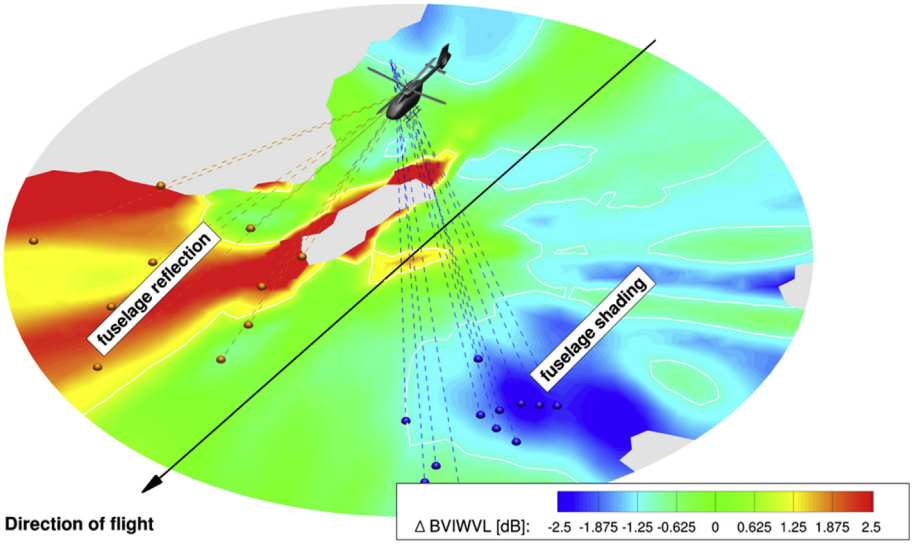

Fig. 3. Influence of the airframe to the BVI assignable noise 4.5 radii below the helicopter (Grey areas excluded due to low overall noise level).

field observers by the Ffowcs-Williams Hawkings based code ACCO, evaluating flow variables on an integration surface encompassing the complete helicopter.

The high-fidelity simulation ensures a precise recording of vortex generation and preservation until its subsequent interaction with the following rotor blade (Fig. 1). Noise sources emitting in the frequency range of concern can be traced back to BVI events (Fig. 2). Shading, diffraction, and reflection effects of the airframe influencing the noise radiation in lateral direction are notable (Fig. 3). Comparing the PNLT time history to flight test data shows very good agreement in shape and absolute values (Fig. 4). The simulation is predominantly located between the rotors' noise (MR + TR signal) and the overall noise (total signal), which includes broad-band and mechanical noise. EPNL values for all microphones show excellent

Please cite this article in press as: A.G. Wilson, Aeroacoustics research in Europe: The CEAS-ASC report on 2016 highlights, Journal of Sound and Vibration (2018), https://doi.org/10.1016/j.jsv.2017.10.016

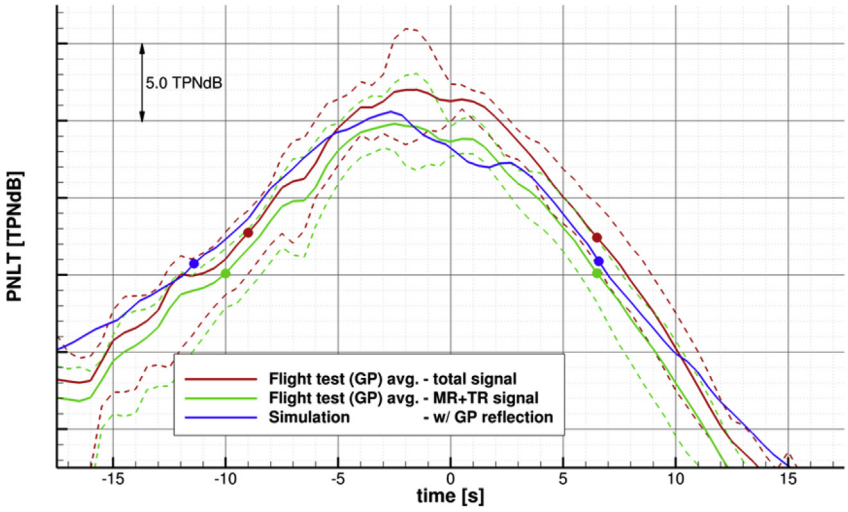

Fig. 4. Comparison of PNLT time history of the center microphone.

consistency within the variance of individual flight tests.

Submitted by U. Schäferlein (schaeferlein@iag.uni-stuttgart.de), M. Keßler and E. Krämer, Institut für Aerodynamik und Gasdynamik, University of Stuttgart.

3.1.2. Experimental investigations on noise shielding by unconventional aircraft configurations

The experimental evaluation of the noise shielding characteristics of unconventional aircraft configurations requires the use of a well-known acoustic source which can be used effectively in a wind tunnel environment (Fig. 5). The latter poses big challenges on wind tunnel setups to avoid the occurrence of any spurious effects related to flow interactions with the source.

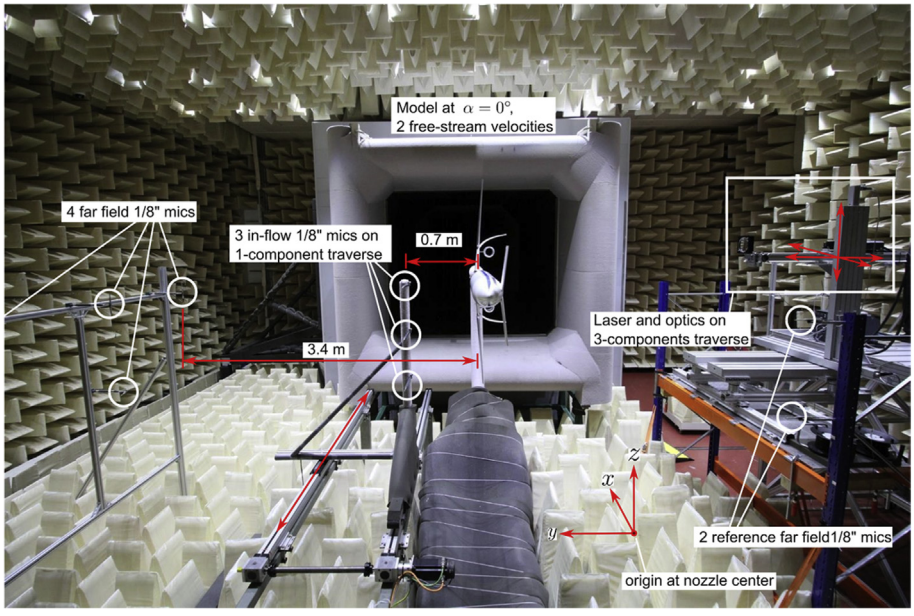

Fig. 5. Experimental setup in the DNW-NWB wind tunnel.

This is especially true when performing experiments in large wind tunnels (Fig. 5), where source installation is often cumbersome. DLR's strategy is to realize a laser-based non-intrusive point source [2–5], effectively circumventing the above limitations of conventional reference noise sources. Furthermore, its properties can be derived directly from the wave equation. Thus, an exact numerical replication of the sound source is possible [4]. The laser-based sound source setup is shown in Fig. 6. A conventional PIV Nd:YAG laser with an output energy of 120 mJ is utilized in combination with custom-

Please cite this article in press as: A.G. Wilson, Aeroacoustics research in Europe: The CEAS-ASC report on 2016 highlights, Journal of Sound and Vibration (2018), https://doi.org/10.1016/j.jsv.2017.10.016

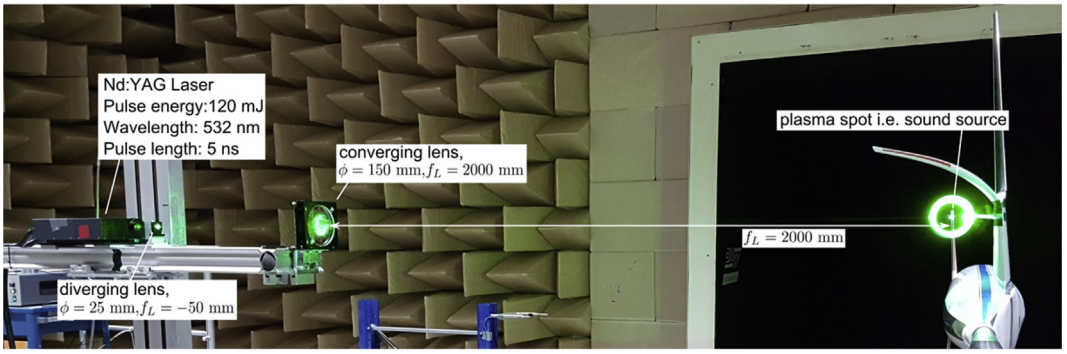

Fig. 6. Schematic view of the laser-based reference sound source.

made optical components to create a plasma spot in the air which acts as the source of sound. The laser-based sound source has a broadband spectrum and a uniform directivity.

An extensive noise shielding database (Fig. 7) was acquired for three aircraft models, DLR's Low Noise Aircraft (Fig. 7a), a Hybrid Wing Body configuration (Fig. 7b) and DLR's F17E UCAV model (Fig. 7c). This data will help validate DLR's numerical simulation methods (ray tracer SHADOW, fast multipole wave solver FMCAS), and will be used for the formulation of low-noise aircraft

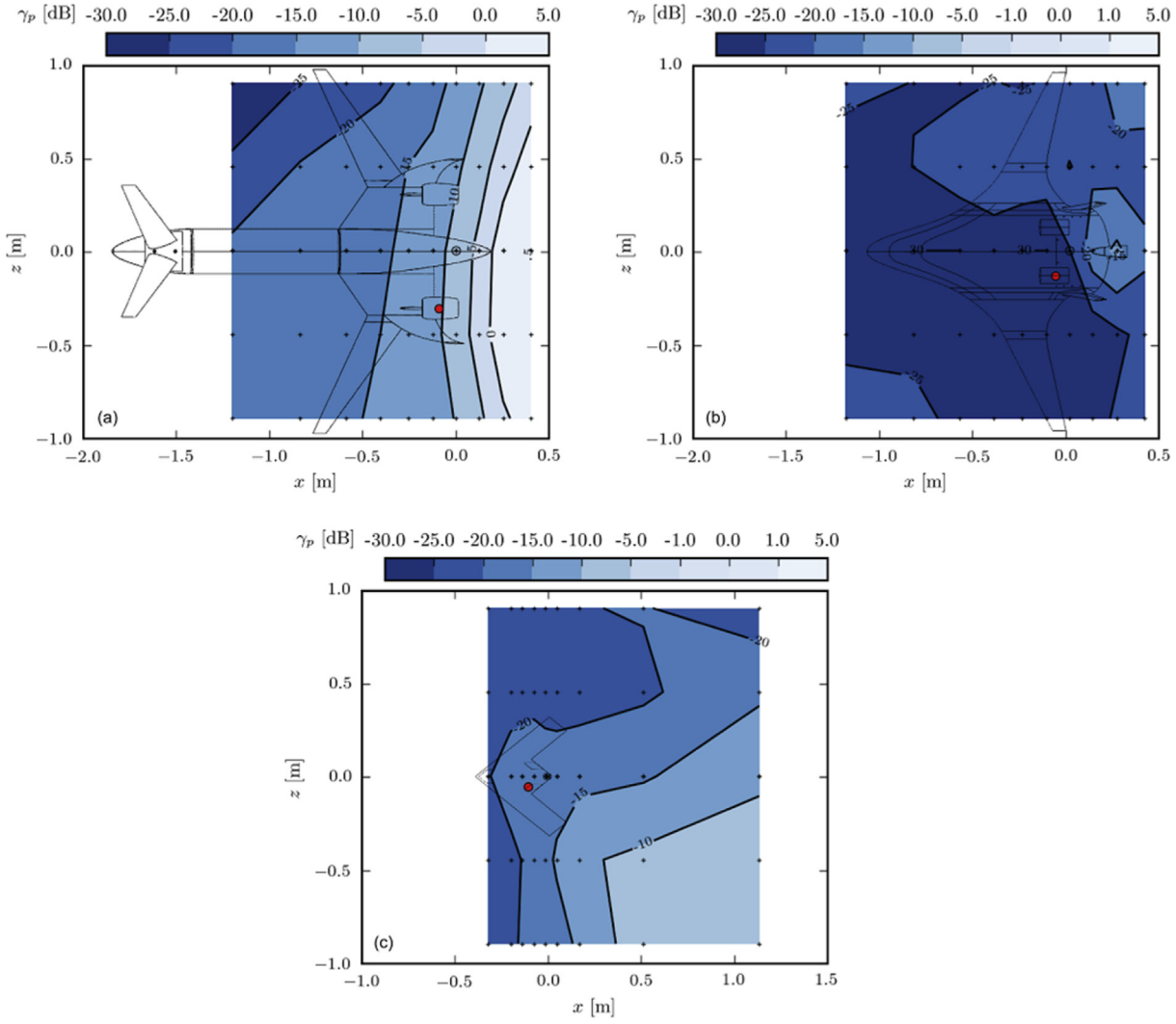

Fig. 7. Contour plots of the overall shielding factor, γ_p [4], for (a) DLR's Low Noise Aircraft configuration, (b) a Hybrid Wing Body configuration and (c) DLR F17E UCAV model. The source location is indicated by the red dots. U_0 = 0 m/s, angle of attack $\alpha = 0°$. (For interpretation of the references to colour in this figure legend, the reader is referred to the Web version of this article.)

Please cite this article in press as: A.G. Wilson, Aeroacoustics research in Europe: The CEAS-ASC report on 2016 highlights, Journal of Sound and Vibration (2018), https://doi.org/10.1016/j.jsv.2017.10.016

design guidelines. This is an important step for the further development of a complete aircraft low noise design capability.

Submitted by K-S. Rossignol (karl-stephane.rossignol@dlr.de) and J Delfs, DLR Institute of Aerodynamics and Flow Technology, Braunschweig, Germany.

3.1.3. Mitigation of pusher-propeller interaction noise by pylon trailing-edge blowing

Pylon-mounted pusher propellers generate extra noise compared to isolated propellers due to the unsteady interaction of the propeller with the pylon wake [6]. An experiment was performed at the Large Low-Speed Facility of the German-Dutch wind tunnels (Fig. 8) to quantify the effectiveness of pylon trailing-edge blowing to reduce the adverse installation effects [7]. This work constituted the first comprehensive experimental analysis of the effects of pylon trailing-edge blowing on the performance and noise emissions of a semi-installed pusher propeller.

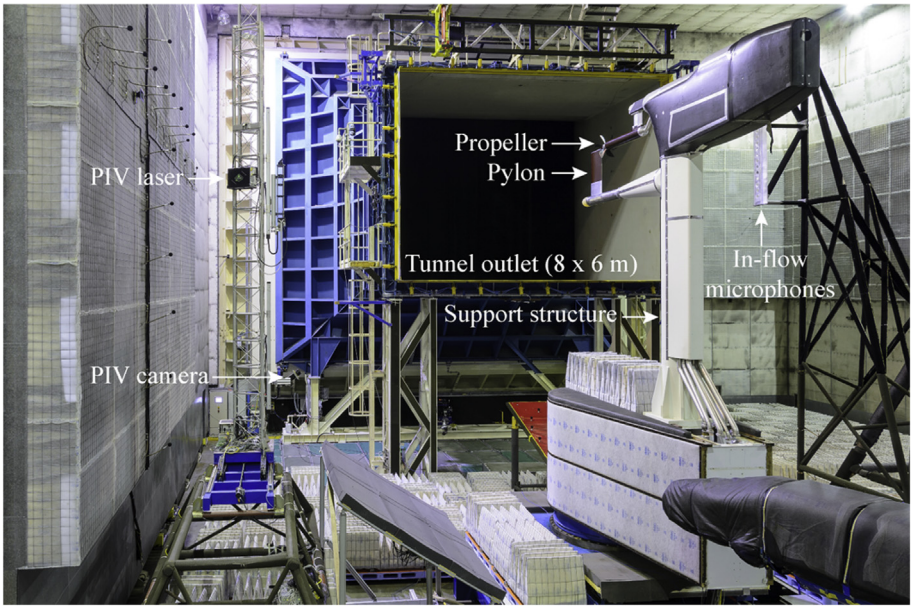

Fig. 8. Pylon–propeller setup in the Large Low-Speed Facility of the German–Dutch wind tunnels.

Particle-image-velocimetry measurements between the pylon and running propeller showed that the blowing system reduced the integrated wake velocity deficit by up to approximately 75% (Fig. 9). The deficit was not completely eliminated due to the limited mixing length between blowing outlet and propeller plane. The blown pylon wake posed a smaller perturbation to the propeller than the wake of the unblown pylon. Consequently, the root-mean-square of the blade load fluctuations was decreased by about 60% at the optimal blowing setting (Fig. 10).

The unsteady blade loads resulting from the pylon-wake encounter caused a tonal-noise penalty of up to 16 dB for the unblown pylon-installed configuration when compared to the isolated propeller. This noise penalty increased with decreasing propeller thrust, and displayed a maximum in the upstream direction. Application of the blowing system at the

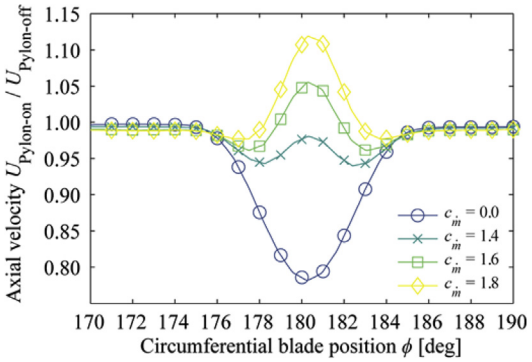

Fig. 9. Reduction of the velocity deficit in the pylon wake at 0.08D upstream of the propeller by blowing. Markers displayed at one-degree intervals for clarity.

Please cite this article in press as: A.G. Wilson, Aeroacoustics research in Europe: The CEAS-ASC report on 2016 highlights, Journal of Sound and Vibration (2018), https://doi.org/10.1016/j.jsv.2017.10.016

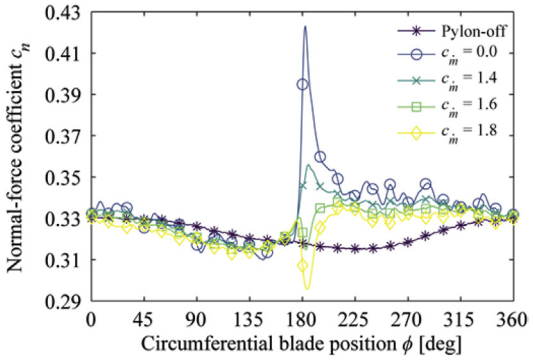

Fig. 10. Reduction of the fluctuations of the unsteady blade normal force by blowing. Markers displayed at fifteen-degree intervals for clarity.

optimal blowing setting eliminated the noise penalty at all but the lowest thrust setting (Fig. 11). Therefore, it is concluded that pylon trailing-edge blowing successfully minimizes the pylon-wake effect occurring for installed pusher propellers.

Submitted by T. Sinnige (T.Sinnige@tudelft.nl), D. Ragni, G. Eitelberg and L. L. M. Veldhuis, Delft University of Technology, The Netherlands.

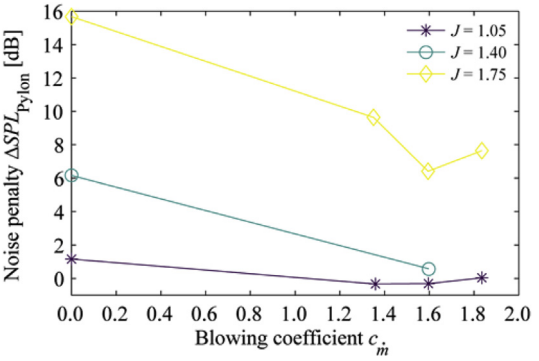

Fig. 11. Reduction of the interaction noise penalty due to pylon installation by blowing.

3.1.4. Empirical model of wall pressure one-point spectra beneath zero and adverse pressure gradient boundary layers

A new model of wall pressure fluctuations including adverse pressure gradient (APG) effects is developed based on five separate experimental investigations covering a large range of Reynolds numbers, see Ref. [8]. From investigations of existing models for APG boundary layers, it is shown that Hu and Herr's (HH) model [9] predicts well the trend of the mid-frequency slope change due to the APG effects and also shows good agreement of the spectral slope at low and high frequencies with the measured spectra. Therefore, HH model is used as the basis for developing the new model. The prediction of the respective

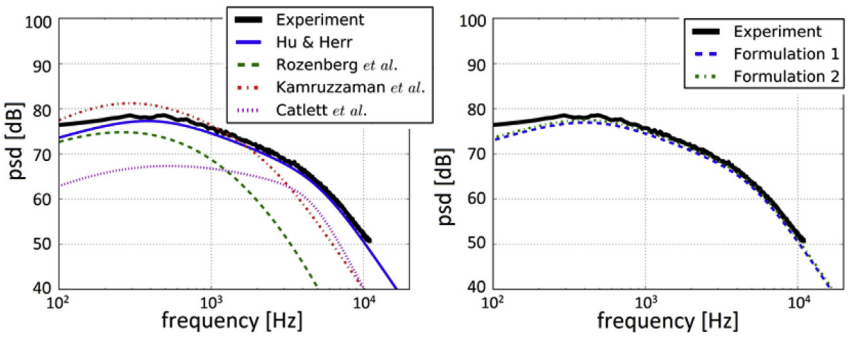

Fig. 12. Predictions of the existing models (left) and the new model (right) for the test case of Hu & Herr [9].

Please cite this article in press as: A.G. Wilson, Aeroacoustics research in Europe: The CEAS-ASC report on 2016 highlights, Journal of Sound and Vibration (2018), https://doi.org/10.1016/j.jsv.2017.10.016

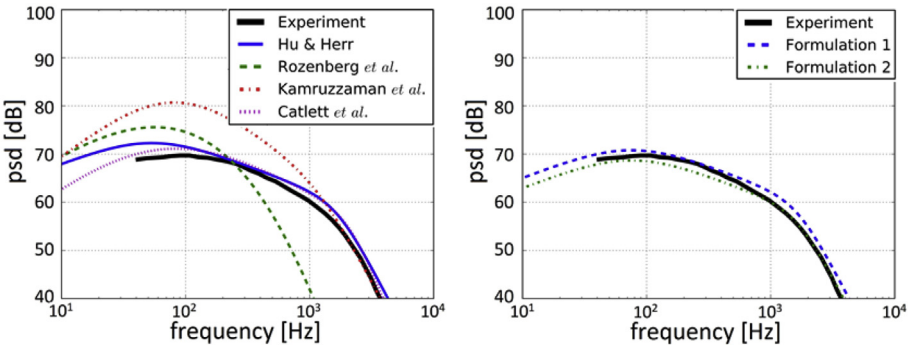

Fig. 13. Predictions of the existing models (left) and the new model (right) for the test case of Catlett et al. [10].

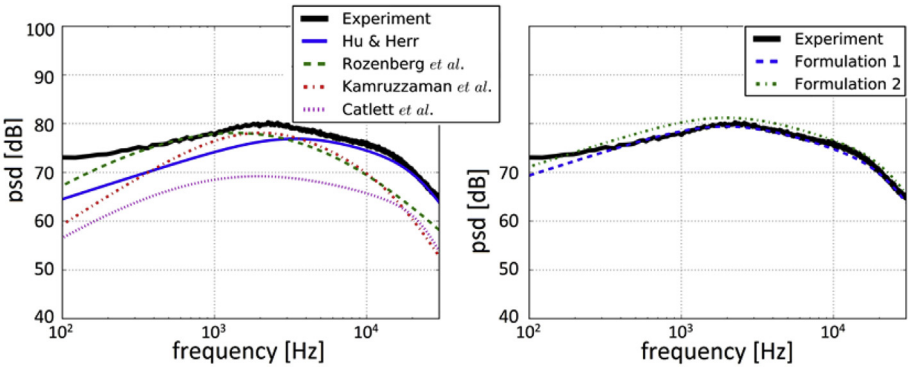

Fig. 14. Predictions of the existing models (left) and the new model (right) for the test case of Suryadi & Herr [11].

spectral location and level is improved by the new model compared to HH model. Two formulations of the new model are proposed. The first formulation uses the momentum thickness Reynolds number (Re_theta) and the boundary layer shape factor to scale the spectral peak level. The second formulation uses a universal scaling parameter, which allows the spectral peaks to collapse within about 4 dB for the selected database.

Figs. 12–14 show the predictions from the new model and the existing models for different experimental cases in which the APG flows were realized on a flat plate with an airfoil mounted above [9], a flat model with tapered trailing edge [10] and a DU96-W-180 airfoil [11]. Fig. 15 shows a prediction for a zero pressure gradient boundary layer [9]. The new model's prediction accuracy is good for all the test cases and shows a significant improvement compared to the existing models.

Submitted by Nan Hu (nan.hu@dlr.de), DLR Institute of Aerodynamics and Flow Technology, Braunschweig, Germany.

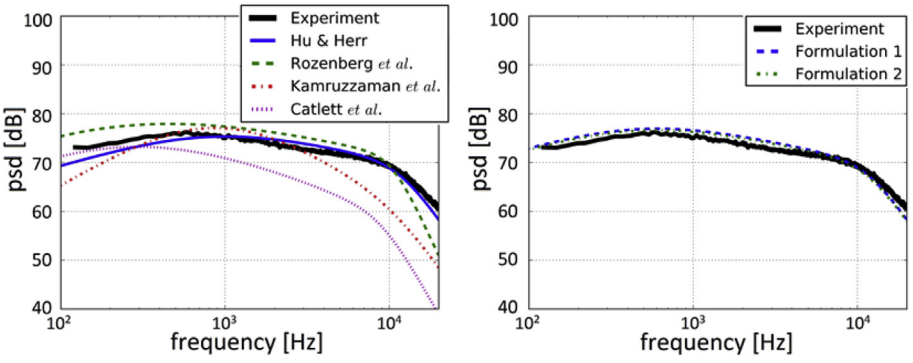

Fig. 15. Predictions of the existing models (left) and the new model (right) for the zero pressure gradient test case of Hu & Herr [9].

Please cite this article in press as: A.G. Wilson, Aeroacoustics research in Europe: The CEAS-ASC report on 2016 highlights, Journal of Sound and Vibration (2018), https://doi.org/10.1016/j.jsv.2017.10.016

3.2. Aeroengine noise (fan and jet)

3.2.1. Investigation of the generation of tones and the feedback loop in supersonic impinging jets using large-eddy simulation

It has been well known for more than sixty years that supersonic jets impinging on a flat plate generate intense acoustic tones due to a feedback loop occurring between the jet nozzle exit and the flat plate, involving aerodynamic disturbances convected downstream in the jet flow and sound waves propagating in the upstream direction. The conditions for the establishment of the loop and the basic nature of the feedback path are however still unclear. They are investigated using large-eddy simulations. Round underexpanded impinging jets are first considered [12]. Snapshots of vorticity fields for these jets are presented in Fig. 16. The generation of tones, and the time variations of the tone intensities, are shown to be linked to

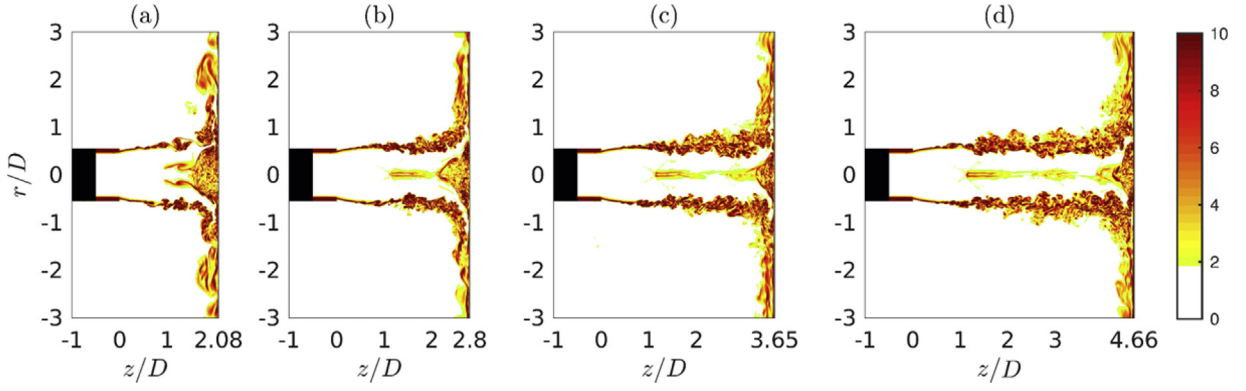

Fig. 16. Snapshots of the normalized vorticity norm obtained for four underexpanded impinging round jets.

the presence and the motions of near-wall shocks inside the jets. Planar and round ideally-expanded impinging jets are then examined [13,14]. The flow and sound fields obtained for such jets are displayed in Fig. 17 and Fig. 18. The results of the

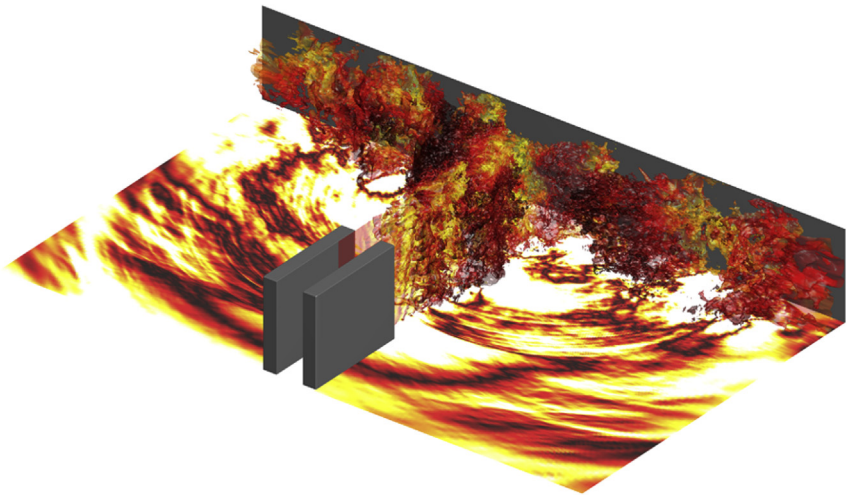

Fig. 17. Representation of isosurfaces of density inside and pressure fluctuations outside the flow of a planar ideally-expanded impinging jet.

simulations are found to be consistent with a modelling of the feedback loop in which the feedback waves are acoustic waves travelling upstream inside the jet flow. These waves are clearly detected in the simulated jets, and characterized from wavenumber-frequency spectra of pressure computed on the jet axis and on the nozzle lip line. These waves appear to belong to the family of the upstream-propagating neutral acoustic wave modes of the jets, see in Fig. 19 the spectrum calculated on the jet axis.

Submitted by Christophe Bogey (christophe.bogey@ec-lyon.fr), Laboratoire de Mécanique des Fluides et d'Acoustique, UMR CNRS 5509, Ecole Centrale de Lyon, France and Romain Gojon, Ecole Centrale de Lyon and Department of Mechanics, Royal Institute of Technology (KTH), Stockholm, Sweden.

Please cite this article in press as: A.G. Wilson, Aeroacoustics research in Europe: The CEAS-ASC report on 2016 highlights, Journal of Sound and Vibration (2018), https://doi.org/10.1016/j.jsv.2017.10.016

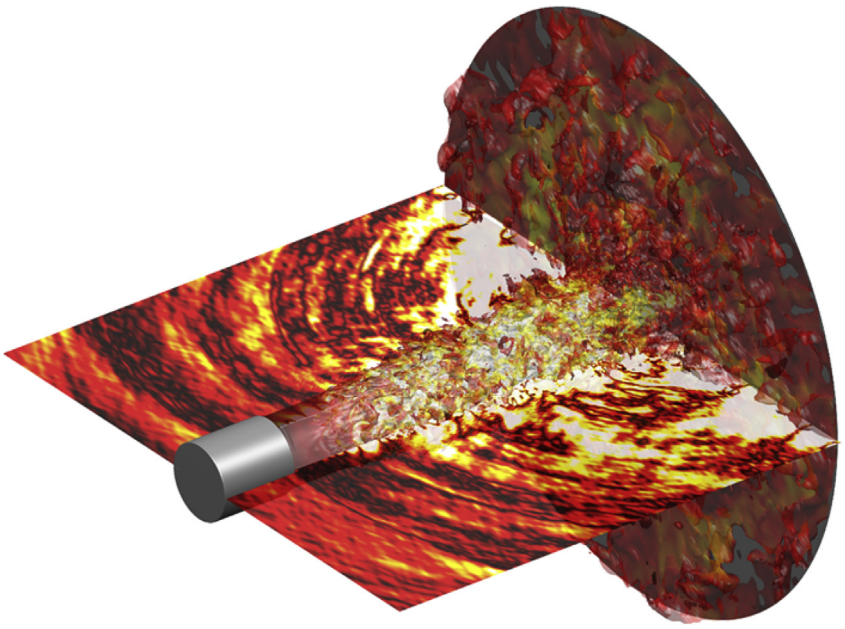

Fig. 18. Representation of isosurfaces of density inside and pressure fluctuations outside the flow of a round ideally-expanded impinging jet.

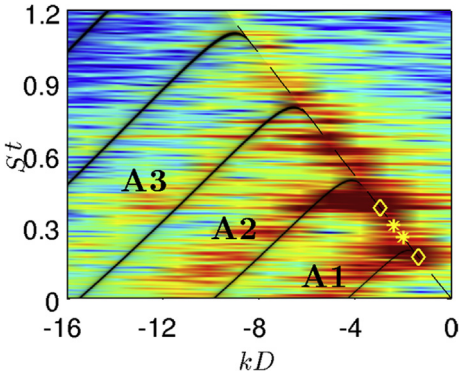

Fig. 19. Frequency-wavenumber spectrum of pressure on the axis of a round ideally-expanded impinging jet; the bands represent the axisymmetric upstream-propagating neutral acoustic wave modes of the jets.

3.2.2. Sound source localization on axial fans using a microphone array method

Microphone array methods are widely used for characterizing aeroacoustic noise sources. For applying beamforming algorithms with deconvolution to axial fans, the rotational motion of the fan, with respect to a stationary microphone array, needs to be compensated. This was done in Ref. [15] for localizing sound sources on an unskewed axial fan at different operating points. The results showed that sound source positions are strongly dependent on the fan operating point and the considered frequency range. In Fig. 20, sound maps of third-octave band with a center frequency of 5 kHz for different flow coefficients PHI, i.e. different operating points, are illustrated. From these sound maps, it is obvious, that sound sources shift from fan blade leading edges to fan blade trailing edges for increasing flow coefficient PHI.

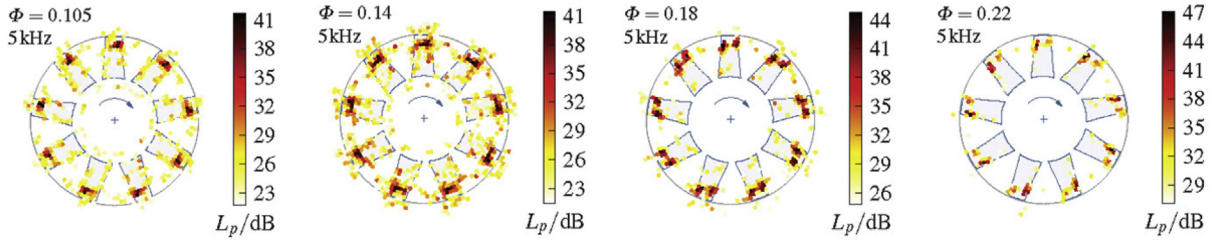

Fig. 20. Sound source maps of third-octave band with center frequency 5 kHz for different flow coefficients PHI [15].

Please cite this article in press as: A.G. Wilson, Aeroacoustics research in Europe: The CEAS-ASC report on 2016 highlights, Journal of Sound and Vibration (2018), https://doi.org/10.1016/j.jsv.2017.10.016

Additionally, sound sources on a backward- and a forward-skewed fan under free and distorted inflow conditions were investigated in Refs. [16,17]. Sound maps of third-octave band with a center frequency of 5 kHz are shown in Fig. 21. For this specific frequency, sound sources for forward-skewed fan shift from fan blade trailing edges to leading edges under distorted inflow conditions. Furthermore, sound source levels for the forward-skewed fan are increased. In contrast to this, sound

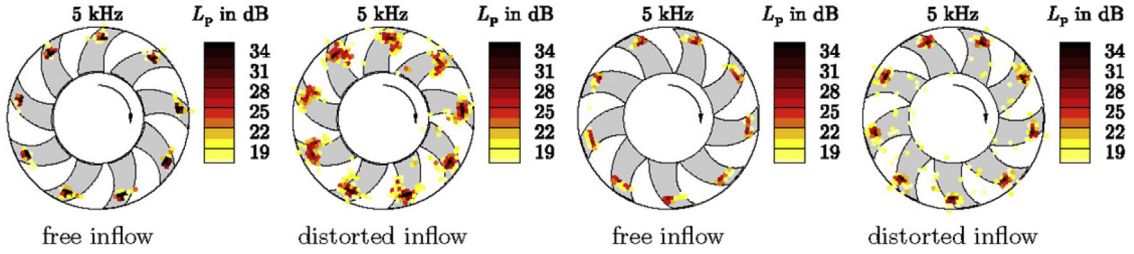

Fig. 21. Sound source maps of third-octave band with center frequency 5 kHz for backward- and forward-skewed fan under free and distorted inflow conditions [17].

source levels of the backward-skewed fan are less affected. Similar observations were made for other third-octave bands. From this and other investigations [18], it was concluded, that sound radiation of forward-skewed fans is more susceptible to distorted inflow conditions, than of backward-skewed fans.

Submitted by Florian Zenger (ze@ipat.uni-erlangen.de)*, Institute of Process Machinery and Systems Engineering, Friedrich-Alexander University Erlangen-Nürnberg, Germany.*

3.2.3. CAA prediction of broadband interaction noise in a turbofan stage using synthetic turbulence

Turbulent flow interactions with the outlet guide vanes are known to mainly contribute to broadband noise emission of aeroengines at approach conditions. Analytical cascade models are used today by Industry but they are limited by the flat-plate assumptions, whereas LES simulations of turbulent sources are generally out of reach of common CFD solvers. An alternative CAA/Euler methodology coupled to a synthetic turbulence inflow has been investigated in recent years by Onera [19]. It is based on a Fourier-mode decomposition of the incoming turbulent wake modeled by an isotropic turbulence energy spectrum and restricted here to the upwash velocity component by analogy with Amiet's theory. 3D simulations are performed using the Onera code *sAbrinA.v0*, solving the linearized Euler equations in the time domain, and applying suited Tam's inflow/outflow boundary conditions (BCs) and periodicity conditions in the azimuthal direction. The fluctuating pressure over the vane surface provided by CAA is used as an input to a Ffowcs-Williams and Hawkings (FWH) integral method to calculate the radiated sound field in the bypass duct. This methodology has been recently extended to full 3D rotor-stator configurations with swirling mean flows and applied to NASA SDT case [20] (see Figs. 22–25). Mean flow convection and turbulence characteristics are provided by RANS and hot-wire measurements too. Sound power level spectra measured by NASA are

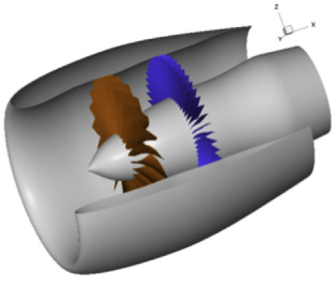

Fig. 22. SDT turbofan model.

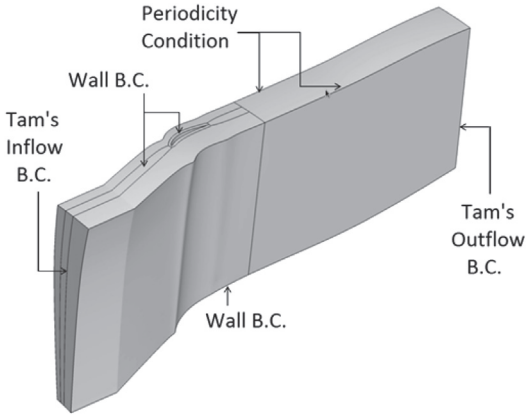

Fig. 23. CAA blocking (1-vane channel) and Boundary Conditions (BCs).

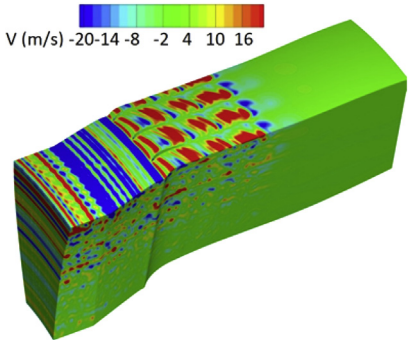

Fig. 24. Turbulent-like velocity snapshot within the CAA domain (3-vane channels).

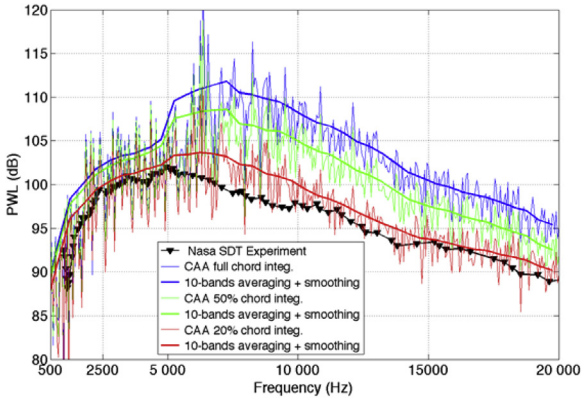

Fig. 25. CAA predictions of PWL spectra (dB) and comparison with experiment.

fairly well assessed by the computations when spurious vorticity-induced wall pressure is removed (practically achieved by limiting the FWH integration to the leading edge region) and when significant cascade effects are accounted for (CAA domain extended to 3-vane channels).

Submitted by C. Polacsek (cyril.polacsek@onera.fr), A. Cader), T. Le Garrec and G. Reboul, ONERA, Châtillon, France.

3.2.4. Aeroacoustics of propulsion systems

In the course of the joint ANR (Agence Nationale de la Recherche)-Safran Aircraft Engines industrial Chair ADOPSYS, aeroacoustics of aeronautical propulsion systems has been studied at Ecole Centrale de Lyon. The three main themes have

Please cite this article in press as: A.G. Wilson, Aeroacoustics research in Europe: The CEAS-ASC report on 2016 highlights, Journal of Sound and Vibration (2018), https://doi.org/10.1016/j.jsv.2017.10.016

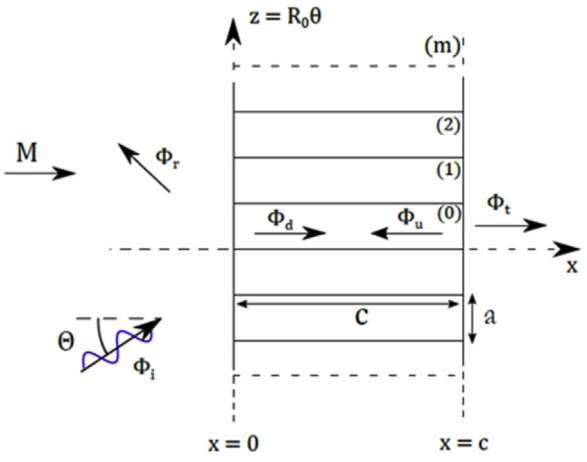

Fig. 26. Turbofan noise: Mode-matching in bifurcated wave guides for noise transmission. Model framework.

been turbofan noise, Counter-Rotating Open Rotor (CROR) noise and jet noise, with the objectives to gain better understanding of the noise sources, better modeling techniques for them and finally propose reduction strategies.

One of the key results for turbofan noise has been the development of a new approach for modeling both noise generation and propagation in a blade row, which could provide an alternative to the already developed strip theory with a 3D rectilinear cascade response obtained by a Wiener-Hopf method [21]. The formulation has been implemented for both incident acoustic waves (sketched in Fig. 26) and vorticity waves (representative of rotor-wake gusts) on outlet guide vanes [22,23]. It can take into account both a slowly varying inter-vane channel (as seen in Fig. 27) and an actual 3D cylindrical geometry without resorting to strips, and it therefore naturally accounts for radial mode scattering. An example of propagation of the mode −12 in the reference NASA-SDT configuration (54 stator vanes) at midspan is shown in Fig. 27 for the approach condition (axial Mach number 0.4). It correlates very well with previous numerical results of Hixon without the spurious reflections at the outlet [24].

Submitted by S. Moreau (stephane.moreau@ec-lyon.fr) and M. Roger, Ecole Centrale de Lyon, Ecully, France.

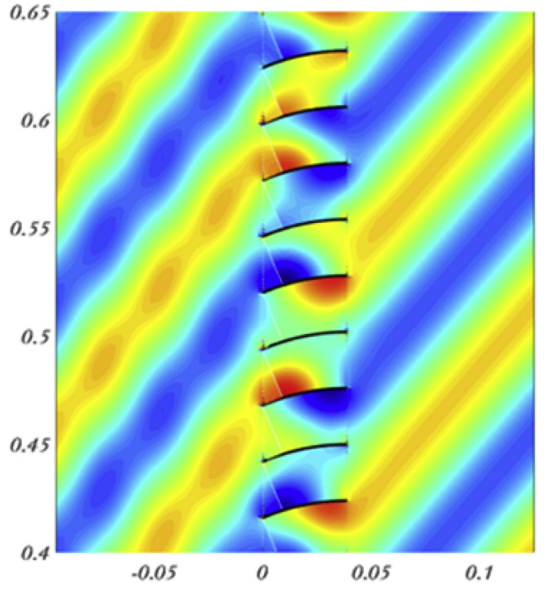

Fig. 27. Turbofan noise: Mode-matching in bifurcated wave guides for noise transmission. Results.

Please cite this article in press as: A.G. Wilson, Aeroacoustics research in Europe: The CEAS-ASC report on 2016 highlights, Journal of Sound and Vibration (2018), https://doi.org/10.1016/j.jsv.2017.10.016

3.3. Airfoil noise (airframe wing and wind turbine)

3.3.1. Low-noise technologies for wind turbine blades

Broadband trailing-edge scattering noise (TEN) represents a canonical source mechanism that occurs in a wide range of technical situations like the noise generation in aircraft high-lift systems, turbomachinery components, cooling fans or wind turbine blades. In modern wind turbines TEN generated in the outer 20–25% of the rotor radius constitutes the most relevant noise contributor.

The German national wind energy project BELARWEA (BMWi ref. 0325726) aims at the development and validation of improved methods to support the design of both efficient and low-noise wind turbine rotors [25]. 2D CFD/CAA-based

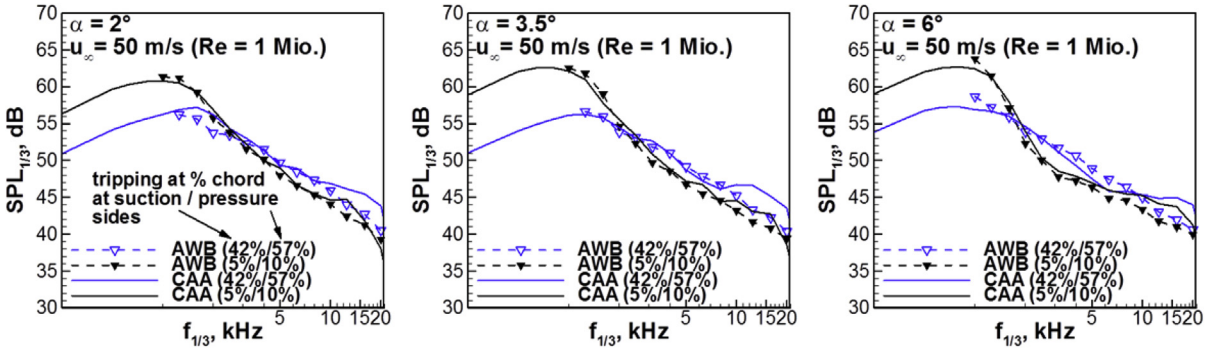

Fig. 28. Comparison of CAA predictions with results from measurements at a 2D RoH-W-18%c37 blade section in the Acoustic Wind-Tunnel Braunschweig (AWB).

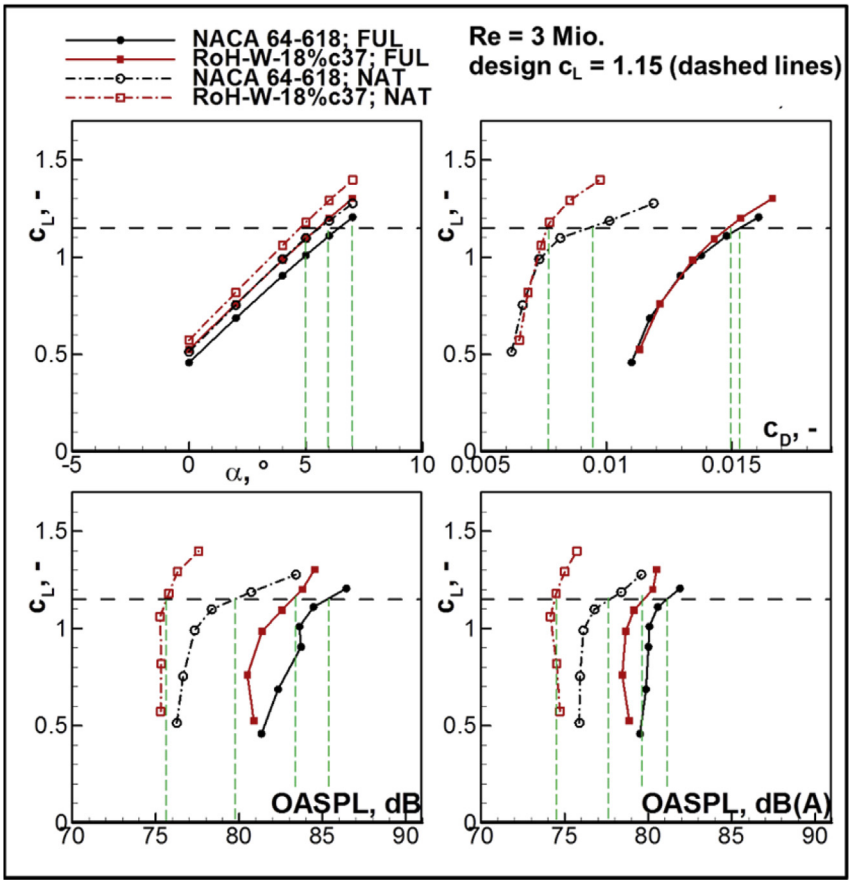

Fig. 29. Predicted aeroacoustic performance of the RoH-W-18%c37 compared to the NACA 64–618 reference for operational conditions, analysis for the cases 'FUL' (fully turbulent boundary-layer from the leading edge) vs. 'NAT' (natural boundary layer transition).

Please cite this article in press as: A.G. Wilson, Aeroacoustics research in Europe: The CEAS-ASC report on 2016 highlights, Journal of Sound and Vibration (2018), https://doi.org/10.1016/j.jsv.2017.10.016

predictions with 4D stochastic source reconstruction using the Fast Random Particle-Mesh Method (FRPM) [26] [27] were successfully applied to predict the TEN emission of a newly designed wind turbine blade profile RoH-W-18%c37. Corresponding validation results are shown in Fig. 28 for varying test angles-of-attack and turbulent boundary-layer transition locations.

When transposing these results to approximate operational conditions (here: to conditions at the outer rotor portion of a small-scaled experimental turbine), the new airfoil design is expected to bring about an overall 2–4 dB TEN reduction when compared to a NACA 64–618 reference profile, cf. Fig. 29.

The noise emission of such an aeroacoustically driven design can be further significantly reduced by the adaptation of TEN reduction concepts known from aerospace-related studies (porous, slotted or brush-type extensions) to the new application conditions [28], see Fig. 30. Compared to standard trailing-edge serrations as currently applied to todays' wind turbine rotors,

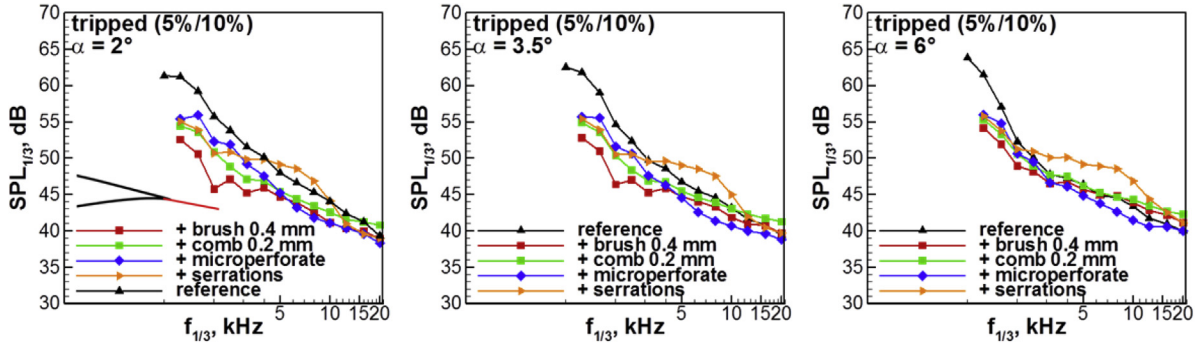

Fig. 30. Effect of selected trailing-edge extensions on TEN spectra for the RoH-W-18%c37. AWB measurement results for conditions as in Fig. 28.

the proposed concepts appear less susceptible to excess noise generation.

Submitted by M. Herr (michaela.herr@dlr.de), R. Ewert, B. Faßmann, C.-H. Rohardt, A. Suryadi, DLR Institute of Aerodynamics and Flow Technology, Braunschweig, Germany, C. Rautmann, Nordex Energy GmbH, Germany and S. Martens, Leibnitz Universität Hannover, Germany.

3.3.2. A numerical approach to trailing edge noise reduction by porous materials

The application of rigid porous materials to airfoils to achieve a reduction of the turbulent boundary layer trailing edge noise was shown experimentally by Herr et al. [29]. Over the past years, numerical methods have been developed to approach this subject in Computational Aeroacoustics (CAA) simulations. Here, Faßmann et al. [30] introduced a volume-averaging description of solid porous permeable materials like metal foams. In the following, it was shown that this approach needs an explicit treatment of the discontinuous interface between the porous material and the surrounding flow. Here, a set of acoustic jump conditions was formulated by Rossian et al. [31] that are based on classic conserved quantities.

In a two-step CFD-CAA simulation framework with DLR's CAA code PIANO enhanced by the treatment for porous materials simulations of a NACA0012 airfoil with a trailing edge made of porous materials starting at 88.75% chord length were run. The beneficial influence of porous materials was shown to be in good accordance with the experimental results. Furthermore, the effect of anisotropic as well as non-uniform materials was studied. Particularly, it was found that the application of non-uniform materials, as shown in Fig. 31, yields a notable noise reduction potential. This is illustrated in Figs. 32 and 33,

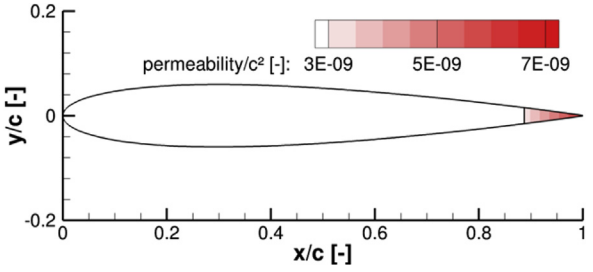

Fig. 31. Sketch of a NACA0012 airfoil with a non-uniform porous permeable trailing edge. The permeability of the material increases linearly towards the trailing edge.

Please cite this article in press as: A.G. Wilson, Aeroacoustics research in Europe: The CEAS-ASC report on 2016 highlights, Journal of Sound and Vibration (2018), https://doi.org/10.1016/j.jsv.2017.10.016

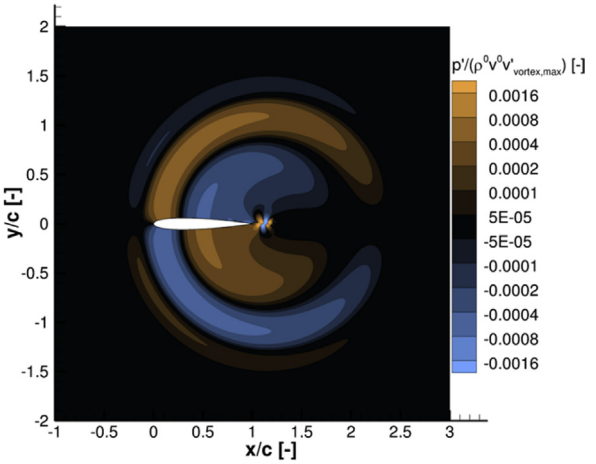

Fig. 32. Snapshot of the normalized acoustic pressure field of the trailing edge noise generated by a single convecting vortex on a NACA0012 airfoil with solid trailing edge.

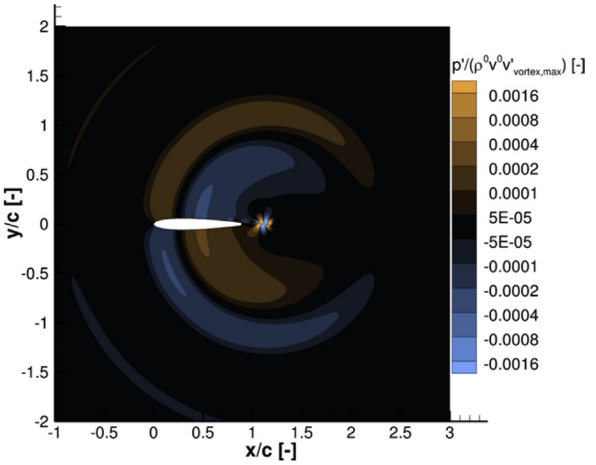

Fig. 33. Snapshot of the normalized acoustic pressure field of the trailing edge noise generated by a single convecting vortex on a NACA0012 airfoil with non-uniform porous trailing edge.

which show one snapshot in time of the acoustic pressure from a simulation with a single Gaussian vortex passing the airfoil with solid or porous trailing edge. Details and further analysis are presented in Ref. [32].

*Submitted by Lennart Rossian (*lennart.rossian@dlr.de*), Roland Ewert and Jan W. Delfs, DLR, Germany.*

3.3.3. Noise reduction mechanism of serrated-trailing-edge devices

Trailing-edge serrations are noise reduction add-ons used mostly in wind-turbine applications. Measurements with microphone arrays reported noise reductions up to 6 dB for flow-aligned serrations retrofitted to a symmetric NACA 0018 airfoil installed in an open-jet wind-tunnel [33] (Fig. 34). Differently, for flow-misaligned serrations retrofitted to symmetric airfoils, noise increase at frequencies higher than the crossover frequency was observed. Similar noise reduction intensities

Please cite this article in press as: A.G. Wilson, Aeroacoustics research in Europe: The CEAS-ASC report on 2016 highlights, Journal of Sound and Vibration (2018), https://doi.org/10.1016/j.jsv.2017.10.016

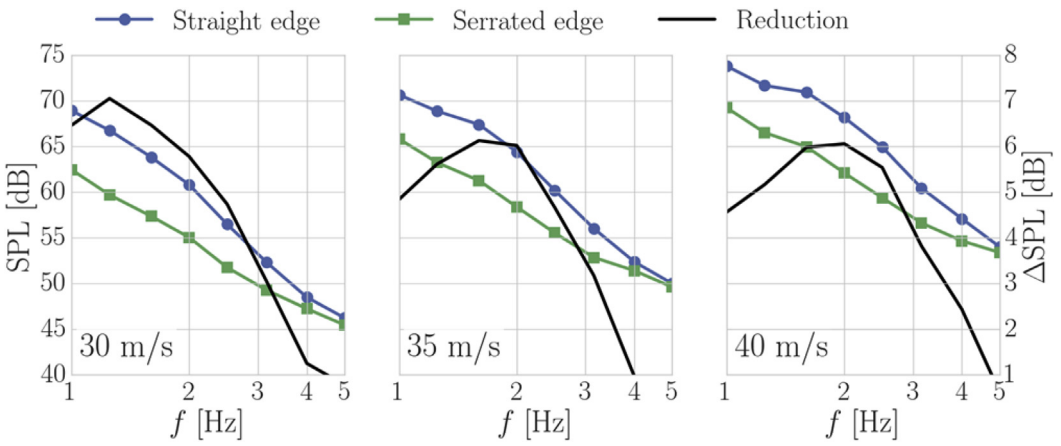

Fig. 34. Acoustic frequency spectra of NACA 0018 airfoil with straight and serrated edges. The SPL reduction is with respect to the straight trailing edge configuration. The angle of attack is 0° [33].

were reported in closed-section wind-tunnel experiments, as well as in numerical computations, where flow-misaligned serrations were installed at the trailing edge of cambered wind-turbine airfoils under high-Reynolds-numbers flows (Fig. 35).

Since the achieved noise reduction depends on the interaction of the incoming turbulent boundary layer with the thin trailing edge, Particle Image Velocimetry (PIV) was also used for its characterization [34] (Fig. 36). By retrieving pressure from velocimetry measurements, it was found that the intensity of the pressure fluctuations varies in the streamwise direction [34]. The largest pressure fluctuations intensity was measured at the root, in the empty space in between serrations. This phenomenon was attributed to the outward and downward flow motions along the serrations [34], later confirmed by the computations with the Lattice-Boltzmann method [35,36]. The latest showed good agreement in terms of noise reductions (Fig. 35), and mean and statistical flow features with respect to the experiments [36]. It was demonstrated that, by choosing the serration geometry aiming at mitigating the flow interaction at the root, larger noise reductions up to 4 dB could be achieved with respect to conventional serrations (Fig. 37) [35,36].

Submitted by R. Merino-Martinez (r.merinomartinez@tudelft.nl), *F. Avallone, D. Ragni and M. Snellen, Faculty of Aerospace Engineering, Delft University of Technology, the Netherlands, W. van der Velden, EXA GmbH, Stuttgart, Germany.*

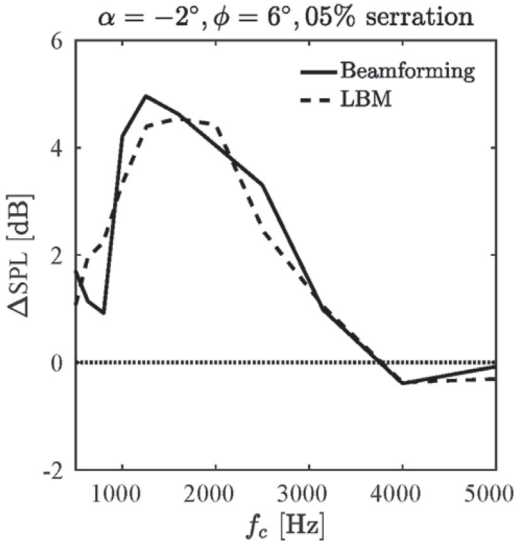

Fig. 35. DELTA SPL of flow-misaligned serrations installed at the trailing edge of a DU96-W-180 airfoil with respect to the straight trailing edge configuration. The angle of attack is -2°. Positive values denote noise reductions.

Please cite this article in press as: A.G. Wilson, Aeroacoustics research in Europe: The CEAS-ASC report on 2016 highlights, Journal of Sound and Vibration (2018), https://doi.org/10.1016/j.jsv.2017.10.016

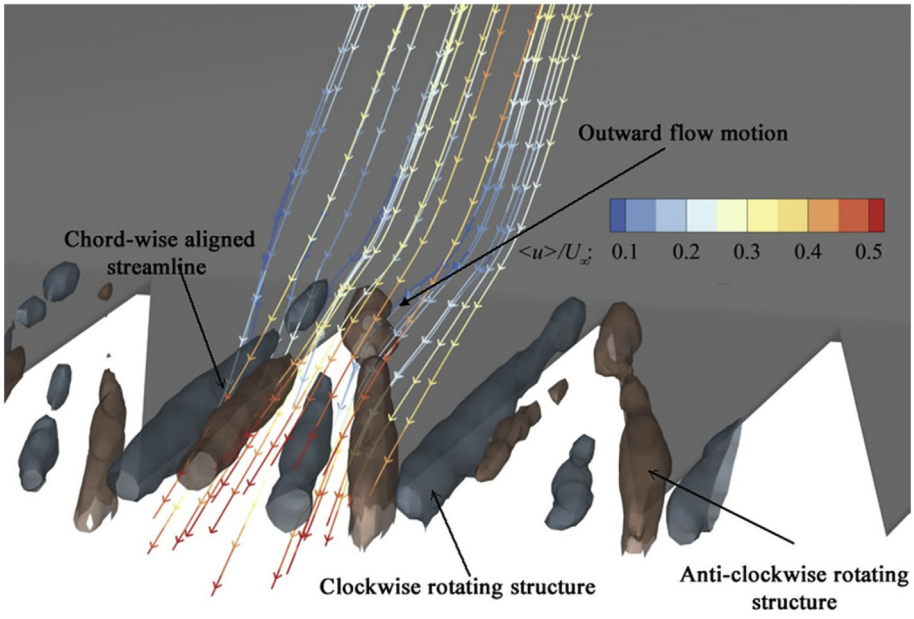

Fig. 36. Mean-flow field over a NACA 0018 with trailing edge serrations [34].

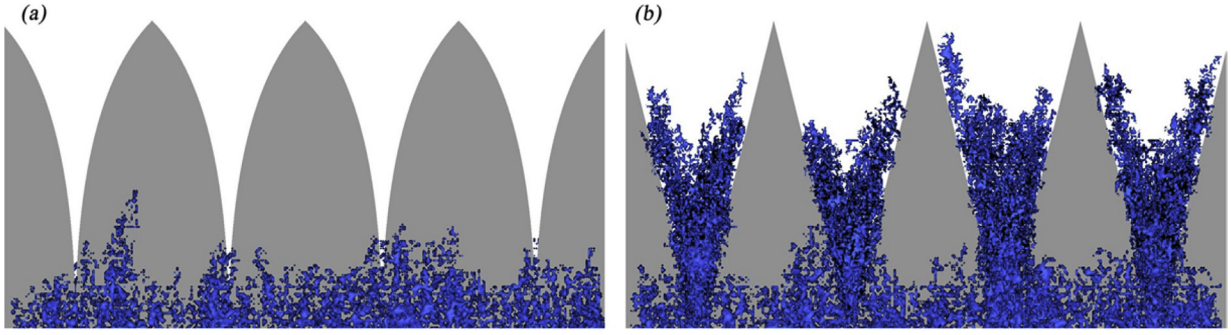

Fig. 37. Iso-surface of noise sources at Strouhal number based on the airfoil chord equal to 4 (f = 400 Hz) for the iron-shaped (a) and sawtooth (b) trailing-edge serrations installed at the trailing edge of a NACA 0018 airfoil.

4. Experimental and numerical methods

4.1. Experimental methods

4.1.1. Aeroacoustic source identification in a confined flow environment using Clustering Inverse Beamforming

Aerodynamic noise is known as the major source of noise at high driving speed. Among the variety of aeroacoustics sources contribution, little is known about car-underbody phenomena.

To tackle the problem of source identification connected to flow confinement, such as hydrodynamic “noise” on microphone array and wall scattering, KU Leuven in collaboration with SIEMENS, designed a quiet noise low speed wind tunnel where a dedicated test rig, reproducing a car-underbody environment, is incorporated (Figs. 38 and 39). A detached-reattached flow on a flexible plate can be generated by means of a horizontal step. A regular array of 45 microphones is

Please cite this article in press as: A.G. Wilson, Aeroacoustics research in Europe: The CEAS-ASC report on 2016 highlights, Journal of Sound and Vibration (2018), https://doi.org/10.1016/j.jsv.2017.10.016

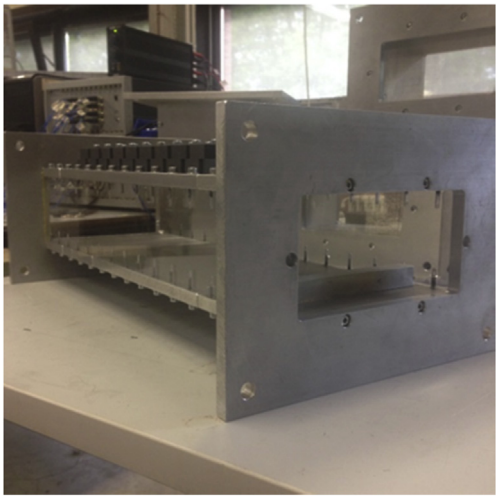

Fig. 38. In sight of detached flow test rig at KU Leuven.

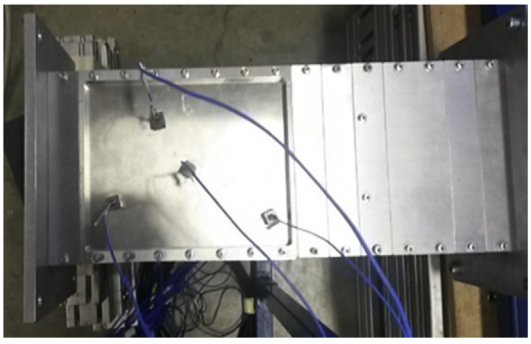

Fig. 39. Detached flow test rig flexible panel configuration.

incorporated in the rigid wall facing the flexible plate, to perform a source identification study adopting the Clustering Inverse Beamforming algorithm (CIB - [37–39]).

CIB is an equivalent source method based on the statistical processing of multiple realizations of the equivalent source field reconstruction with different microphone's array sub-sets (clusters). The source reconstruction is strengthened by defining, in the source region, a weighting function from 0 to 1 expressing the confidence level of finding a physical source in the proximity of a given location.

Encouraging results for the identification of an aeroacoustics source generated by the flow detachment were obtained adopting the radiation model of a monopole in open space (Fig. 40).

Assuming as a radiation model the Green's function of a monopole in a finite length duct [40], we expect to generate an iterative procedure capable of identifying the unknown modal reflection coefficients down-stream and up-stream of the source region and to improve the CIB source identification while keeping the microphone array configuration unchanged.

Submitted by A. Ammirati (antonio.ammirati@kuleuven.be), W. De Roeck and W. Desmet, KU Leuven, C. Colangeli and K. Janssens, Siemens, Belgium.

Please cite this article in press as: A.G. Wilson, Aeroacoustics research in Europe: The CEAS-ASC report on 2016 highlights, Journal of Sound and Vibration (2018), https://doi.org/10.1016/j.jsv.2017.10.016

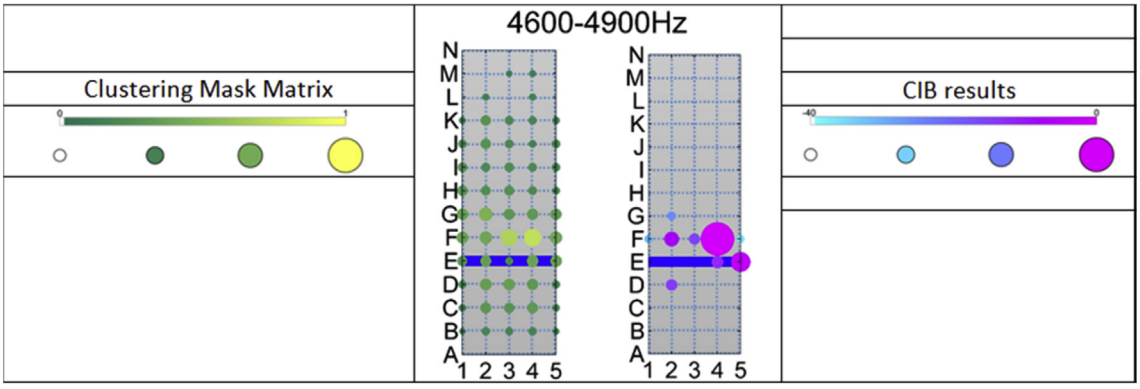

Fig. 40. CIB solution for aeroacoustics source generated by the flow detachment, clustering mask matrix ranges from 0 to 1, equivalent source reconstruction normalized to the maximum with 40 dB of range.

4.1.2. The Strehl-ratio as a measure for the microphone-array efficiency

The Strehl-ratio is a dimensionless quantity, rating the quality of the images of ideal optical point sources on telescopes compared to diffraction limited optical systems [41]. This measure is introduced in the present paper for the characterization of the frequency dependent efficiency of a microphone array. The microphone-array output for an acoustic monopole source in the center of the focal plane is a point spread function (PSF). The PSF depends on the frequency, microphone layout, quality of microphones and signal processing. In case of an inflow array used in wind-tunnels for aeroacoustic measurements, phase errors due to sound propagation in the flow field play a role as well [42]. The ratio of the PSF-peak value compared to the maximum attainable value for an ideal PSF limited only by diffraction over the specific aperture will be defined as the Strehl-ratio. Both peak values are normalized with the Integral of the respective PSF. By this the Strehl-ratio has a value between 0 and 1. An ideal microphone array with infinite numbers of perfect working sensor will have a Strehl-ratio of 1. In a first step the Strehl-ratio is determined numerically and used as a quality criterion in the optimization process of the microphone-array layout (Figs. 41 and 42). In a second step the performance of the manufactured microphone-array is checked by calculating

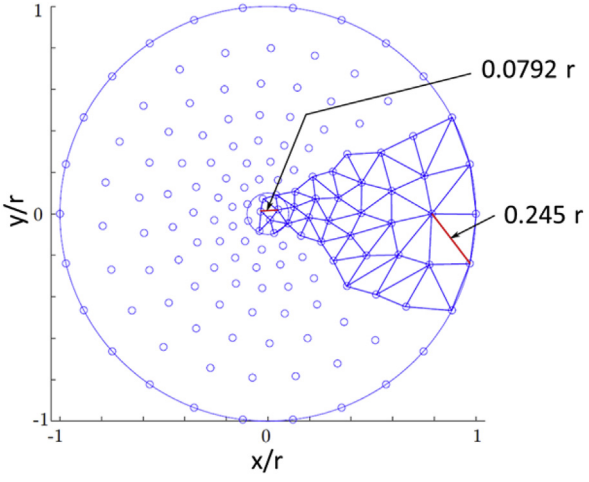

Fig. 41. Final microphone-array layout resulting from a grid-generator. The step size increases linearly with the distance to the center. A number of 144 Sensors are arranged within a radius of r = 0.75 meter.

Please cite this article in press as: A.G. Wilson, Aeroacoustics research in Europe: The CEAS-ASC report on 2016 highlights, Journal of Sound and Vibration (2018), https://doi.org/10.1016/j.jsv.2017.10.016

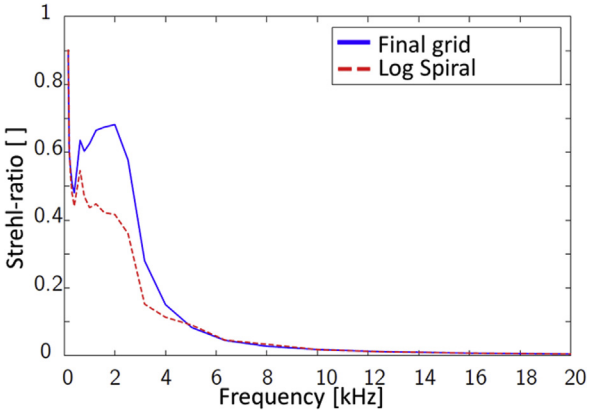

Fig. 42. The frequency dependent Strehl-ratio of the final array-layout compared to results for a sensor arrangement on 9 logarithmic spirals according to Underbrink [43]. The maximum diameter d = 1.5 m and Number of microphones N = 144 is the same in both cases.

the Strehl-ratio from experimental data obtained in wind-tunnel measurements. The numbers are compared to the theoretical results in order to quantify the influence of wind-tunnel effects on the array performance (Fig. 43).

Submitted by K. Ehrenfried (klaus.ehrenfried@dlr.de)*, A. Henning and B. Schmidt, DLR Institute of Aerodynamics and Flow Technology, Göttingen, Germany.*

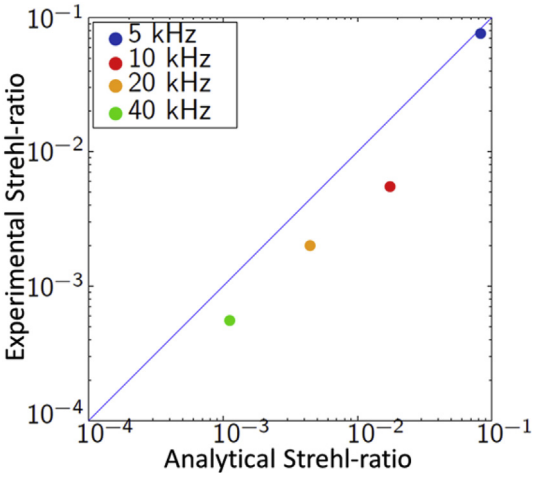

Fig. 43. Frequency dependent Strehl-ratio obtained from measurements in the closed section of a wind-tunnel compared to the theoretical values.

4.1.3. A method for evaluating the characteristic lengths of coherent surface pressure fluctuations with unknown flow direction

Characteristic lengths of the coherent surface pressure fluctuations are required for predictions of aero-vibro-acoustic excitation of aircraft fuselage structures. When determining the characteristic lengths of the coherent pressure it is important to consider the flow direction in order to correctly identify stream-wise and cross-stream directions. In the past, this has either not been considered in flight testing [44] [45], or has been approached in a way that limited the diversity of measurement points taken [46]. In order to overcome these limitations, a method is described for determining the unknown flow direction directly from the surface pressure fluctuation data. In contrary to former experiments where linear arrays were used, a two-dimensional array distribution was implemented on the fuselage of an aircraft. The resulting two-dimensional coherence patterns were evaluated to yield both the characteristic length in the stream-wise (Fig. 44) and cross-stream (Fig. 45) directions and the flow direction (Fig. 46) without prior knowledge or orientation of the transducer array with the flow [47]. The results from the measurements were compared to characteristic lengths from prediction models in order to qualify the models for use at transonic velocities. It was found that predictions from models which had been set up with profound knowledge of the flow direction were considerably closer to the measured data than when the flow direction had

Please cite this article in press as: A.G. Wilson, Aeroacoustics research in Europe: The CEAS-ASC report on 2016 highlights, Journal of Sound and Vibration (2018), https://doi.org/10.1016/j.jsv.2017.10.016

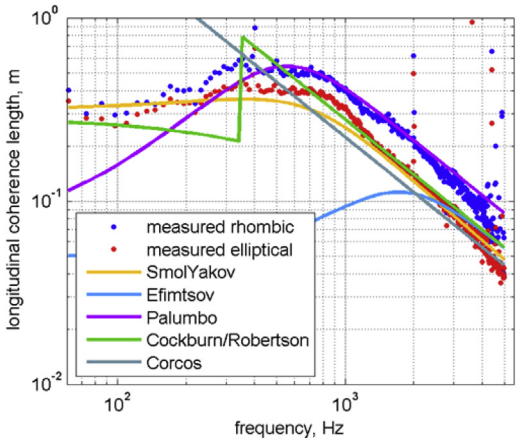

Fig. 44. Measured coherence length in stream-wise direction after consideration of flow angle. Comparison with model predictions.

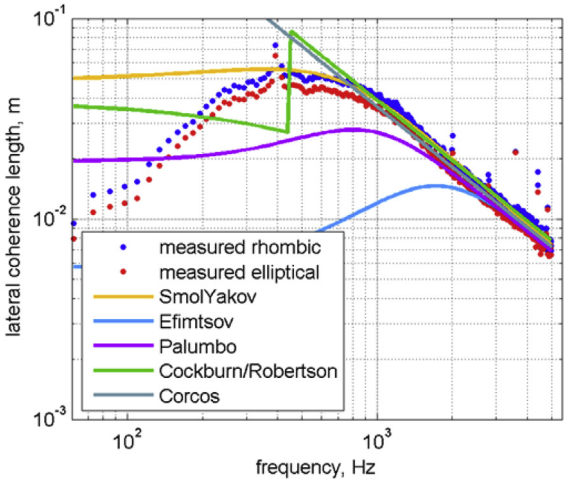

Fig. 45. Measured coherence length in cross-stream direction after consideration of flow angle. Comparison with model predictions.

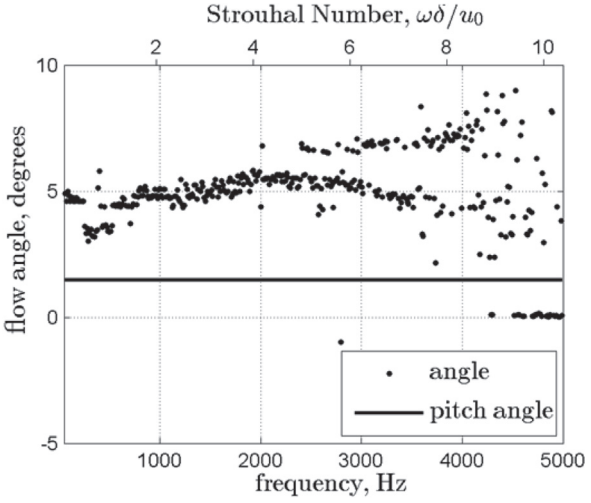

Fig. 46. Flow angle determined from the coherent pressure pattern orientation.

Please cite this article in press as: A.G. Wilson, Aeroacoustics research in Europe: The CEAS-ASC report on 2016 highlights, Journal of Sound and Vibration (2018), https://doi.org/10.1016/j.jsv.2017.10.016

not been considered in the setup of the model. The new method provides a flexible way to overcome the issues of unknown flow direction at any flight attitude.

Submitted by S. Haxter (stefan.haxter@dlr.de) *and C. Spehr, DLR Institute of Aerodynamics and Flow Technology, Göttingen, Germany.*

4.2. Numerical methods

4.2.1. Perturbed Convective Wave Equation for the precise computation of fan noise

For the modeling of aerodynamically generated sound of rotors, the Ffowcs Williams-Hawkings equation is the method of choice to compute noise generated in the presence of moving surfaces [48]. However, we are interested in fully resolving the acoustic field both within the rotating as well as stationary parts and base our physical model on the Acoustic Perturbation Equations (APE) [49]. By assuming the acoustic field to be irrotational, we may introduce the scalar acoustic potential and are able to reformulate APE by a convective wave equation, which we name Perturbed Convective Wave Equation (PCWE). It fully describes acoustic sources generated by incompressible flow structures and its wave propagation through flowing media. The mathematical description is based on an arbitrary Lagrangian–Eulerian framework, and is numerically solved by the Finite-Element (FE) method utilizing a Nitsche-type mortaring between stationary and rotating regions [50]. The applicability of the computational scheme is demonstrated by computing the noise generated by an axial fan. Thereby, the flow field is solved by a Detached Eddy Simulation (see Fig. 47) and the substantial derivative of the incompressible flow pressure defines the acoustic sources (see Fig. 48). Fig. 49 displays the computed power spectral density at the microphone position. Thereby, we display the smoothed measured spectra obtained from the 30s recorded acoustic pressure signal as well as the individual spectra by just using measured data of 0.1s (in grey). The computed spectrum based on our numerical simulation is computed out of a real time simulation of 0.06s.

*Submitted by M. Kaltenbacher (*manfred.kaltenbacher@tuwien.ac.at*) and A. Hüppe, Vienna University of Technology, Austria, F. Zenger and S. Becker, University of Erlangen, Germany.*

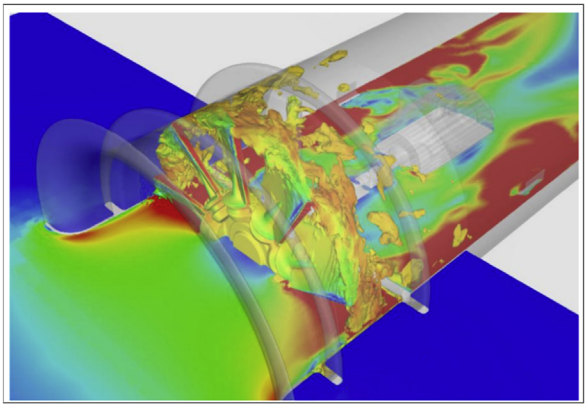

Fig. 47. Flow structure at a characteristic time step.

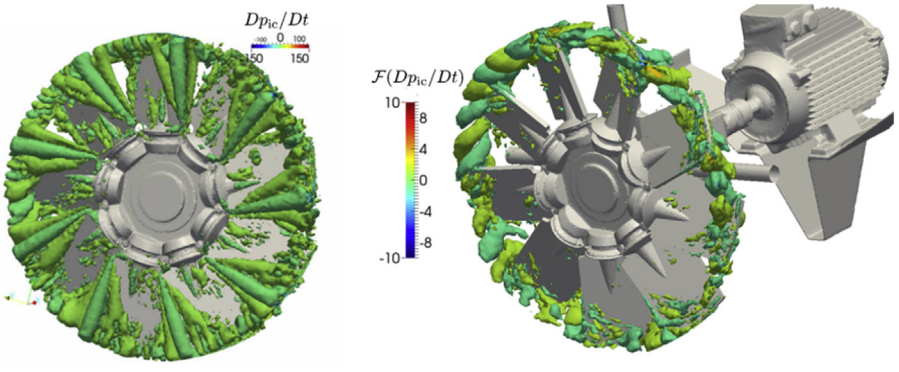

Fig. 48. Structure of acoustic source terms at a characteristic time step and in the frequency domain at 254 Hz.

Please cite this article in press as: A.G. Wilson, Aeroacoustics research in Europe: The CEAS-ASC report on 2016 highlights, Journal of Sound and Vibration (2018), https://doi.org/10.1016/j.jsv.2017.10.016

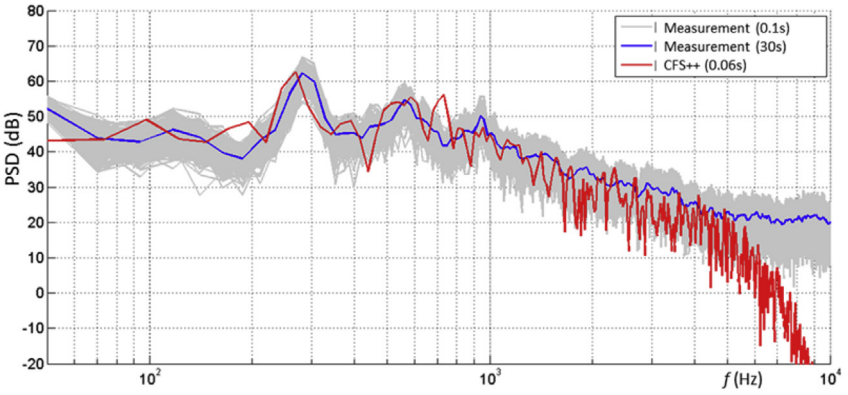

Fig. 49. Spectral density (relative to 20 μPa) of the measured microphone signal and computed acoustic pressure.

4.2.2. Experimental modal decomposition and numerical simulation of the noise produced by an environmental control system including installation effects

In the framework of the FP7 IDEALVENT project coordinated by the von Karman Institute (VKI, Belgium), a number of innovative developments were carried out in order to permit the investigation of aerodynamic and aeroacoustic installation effects in aircraft Environmental Control Systems. The partners worked on 3 typical components that are usually needed in such a system to provide fresh air in the aircraft cabin and to cool down electronic equipment: a blowing unit and a butterfly valve provided by Liebherr Aerospace (France), and a diaphragm. A novel multi-modal source characterization procedure was developed by the Royal Institute of Technology (Sweden), the Catholic University of Leuven (Belgium) and the VKI for the decontamination of in-duct acoustic measurements, removing acoustic reflection and turbulent boundary layer pressure fluctuations effects [51]. The procedure was also applied to scale-resolved Improved Delayed Detached Eddy Simulations (IDDES, Fig. 50, [52]) obtained by New Technologies and Services

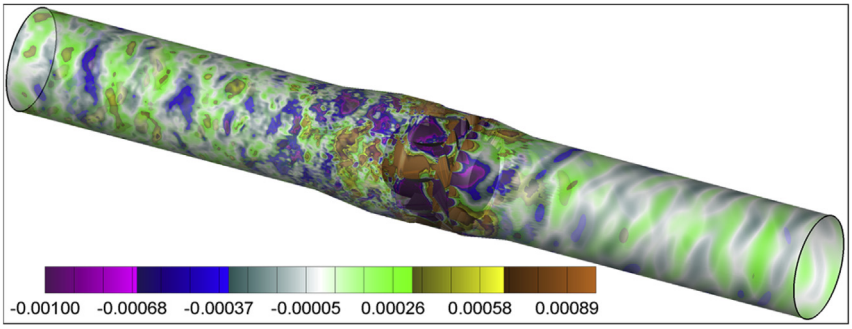

Fig. 50. Instantaneous fields of pressure fluctuations (normalized by the ambient pressure) on duct wall, obtained by IDDES.

(Russia), permitting the unambiguous cross-validation of experimental and numerical results for different inlet geometries leading to different installation effects. The noise produced by the blower unit was also simulated by the German Aerospace Center (Germany) applying their Random Particle Mesh (RPM) stochastic approach (Fig. 51, [53]), Siemens Industry Software (Belgium) using their Finite Element (FE) solver (Fig. 52) and the Ecole Centrale de Lyon (France)

Please cite this article in press as: A.G. Wilson, Aeroacoustics research in Europe: The CEAS-ASC report on 2016 highlights, Journal of Sound and Vibration (2018), https://doi.org/10.1016/j.jsv.2017.10.016

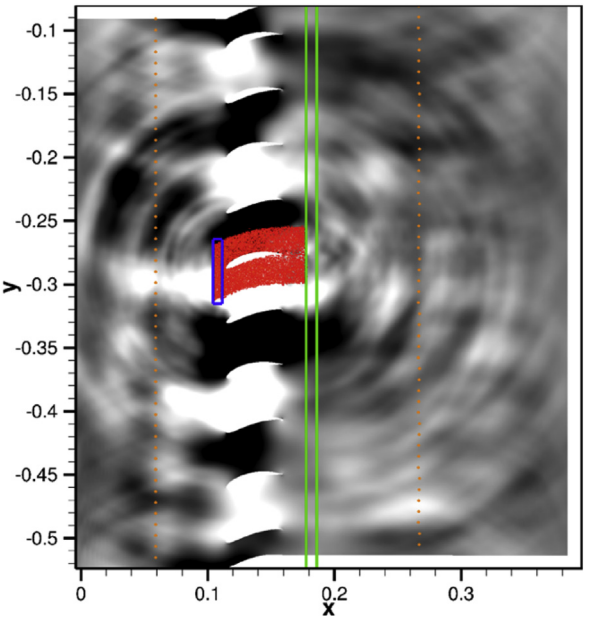

Fig. 51. Setup for the RPM broadband simulations. Blue: inflow patch, green: outflow patch, red: stochastic vorticity fluctuations, grey: instantaneous acoustic pressure. (For interpretation of the references to colour in this figure legend, the reader is referred to the Web version of this article.)

applying an advanced analytical modal matching approach (Fig. 53, [54]).

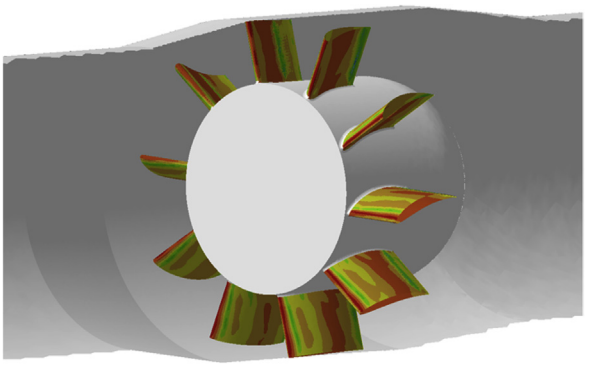

Fig. 52. Dipolar source distribution over the stator vanes in the FE simulation.

Submitted by C. Schram (christophe.schram@vki.ac.be) *and J. Christophe, VKI, Belgium, S. Sack and M. Abom, KTH, Sweden, W. De Roeck and H. Denayer, KUL, Belgium, M. Shur, M. Strelets and A. Travin, NTS, Russia, A. Wohlbrandt, S. Guerin and R. Ewert, DLR, Germany, P. Martinez-Lera and K. Kucukoskun, SISW, Belgium, B. Francois, S. Bouley and M. Roger, ECL, France.*

Please cite this article in press as: A.G. Wilson, Aeroacoustics research in Europe: The CEAS-ASC report on 2016 highlights, Journal of Sound and Vibration (2018), https://doi.org/10.1016/j.jsv.2017.10.016

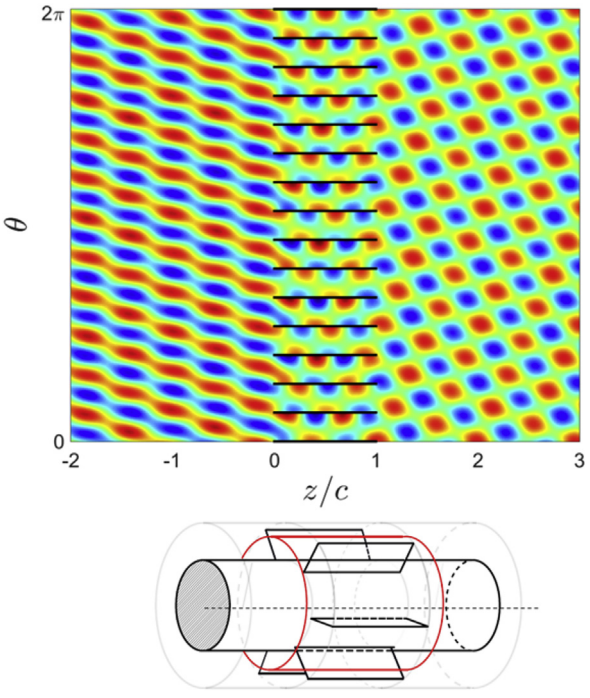

Fig. 53. Instantaneous acoustic pressure field obtained with the mode-matching technique for an oblique acoustic field incident on a blade cascade at zero angle of attack.

4.2.3. Tailored Green's functions for flow noise predictions in ducted diaphragms

The noise produced by single and tandem diaphragms in a duct is studied by means of compressible Large Eddy Simulation (LES), using a hybrid approach based on Lighthill's analogy [55] and using a tailored Green's function for sound generation and radiation in low-Mach number ducted diaphragm flows. The tailored Green's function accounts for the scattering of the equivalent aeroacoustic sources by the duct and diaphragm(s). The scattering by a single ducted diaphragm is obtained using the mode-matching technique proposed by Rienstra [56]. It is combined with a recursive summation of the reflected waves between the two diaphragms, in order to extend the Green's function solution to the tandem diaphragms case. The developed method is limited to low-Mach number flows, as mean flow effects are not accounted for in the proposed procedure. Based on Lighthill's analogy, the equivalent sources are computed using the turbulent velocity fluctuation extracted from the LES, to generate a volume-distributed source field. For the sake of computational efficiency, a grouping scheme based on octree structure is suggested, allowing to decrease the number of point sources without causing a significant loss of accuracy of the predicted acoustic far-field. The results are validated against in-duct aeroacoustic measurements (see Figs. 54–57). Considering the agreement between the predictions and the measurements, the developed approach can be claimed to

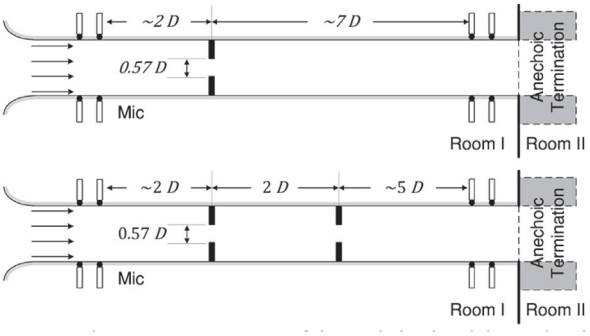

Fig. 54. Schematic representation of the single (top) and the tandem (bottom) diaphragm cases.

Please cite this article in press as: A.G. Wilson, Aeroacoustics research in Europe: The CEAS-ASC report on 2016 highlights, Journal of Sound and Vibration (2018), https://doi.org/10.1016/j.jsv.2017.10.016

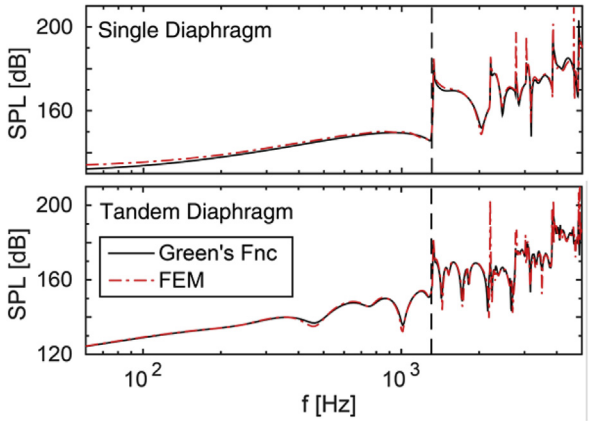

Fig. 55. Validation of the tailored Green's functions for single and tandem diaphragm cases against a commercial numerical solver, investigating the acoustic response of a test quadrupole. The vertical dashed line indicates the first cut-off frequency.

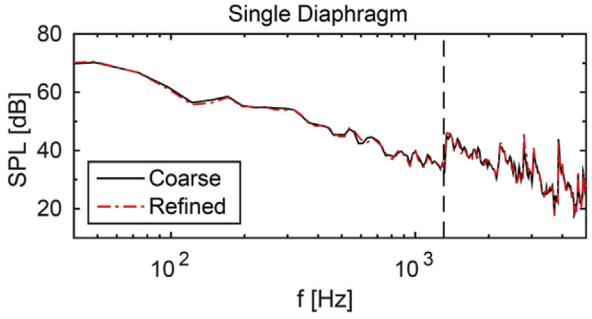

Fig. 56. Comparison of the proposed grouping scheme and the refined scheme for convergence.

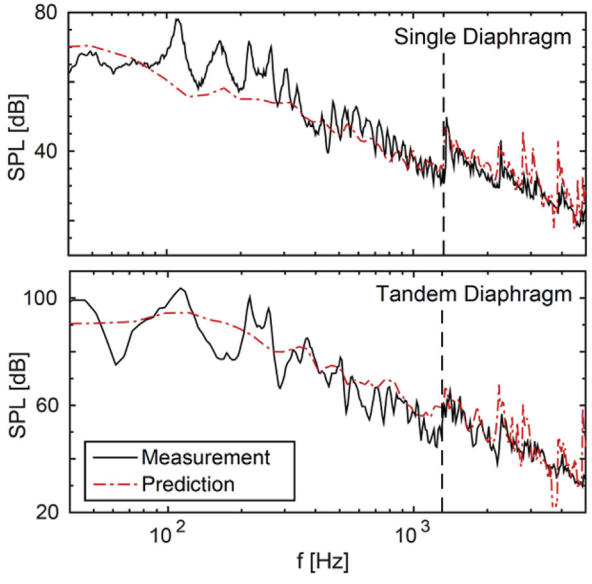

Fig. 57. Comparison of the noise spectra obtained from the measurements and the noise prediction method for the single and the tandem diaphragm cases. The vertical dashed line indicates the first cut-off frequency.

Please cite this article in press as: A.G. Wilson, Aeroacoustics research in Europe: The CEAS-ASC report on 2016 highlights, Journal of Sound and Vibration (2018), https://doi.org/10.1016/j.jsv.2017.10.016

provide robust and accurate solution for noise prediction in low-Mach number ducted diaphragm flows without using any pressure data.

Submitted by U. Karban (ugkarban@gmail.com), C. Schram, von Karman Institute for Fluid Dynamics, C. Sovardi and W. Polifke, Technical University of Munich.

4.2.4. Numerical study of the nonlinear behavior of passive absorbers

Acoustic damping systems, such as Helmholtz resonators, perforated liners, or quarter wavelength cavities are commonly used in multiple industrial applications to reduce noise or control thermoacoustic instabilities [57]. Linear and nonlinear dissipation mechanisms involved differ significantly depending on the amplitude of the acoustic excitation due to flow separation effects.

The present work investigates the physics of Helmholtz resonators under a large range of excitation amplitudes and frequencies applying two different CFD simulations approaches: a compressible simulation of the whole resonator [58] and an approach based on resonator decomposition combined with incompressible simulations [59]. The excitation amplitudes have to be adjusted such that the flow conditions within the neck accord for both approaches. The determined resonator impedances by both approaches agree well and are validated against experiments. The decomposed incompressible approach

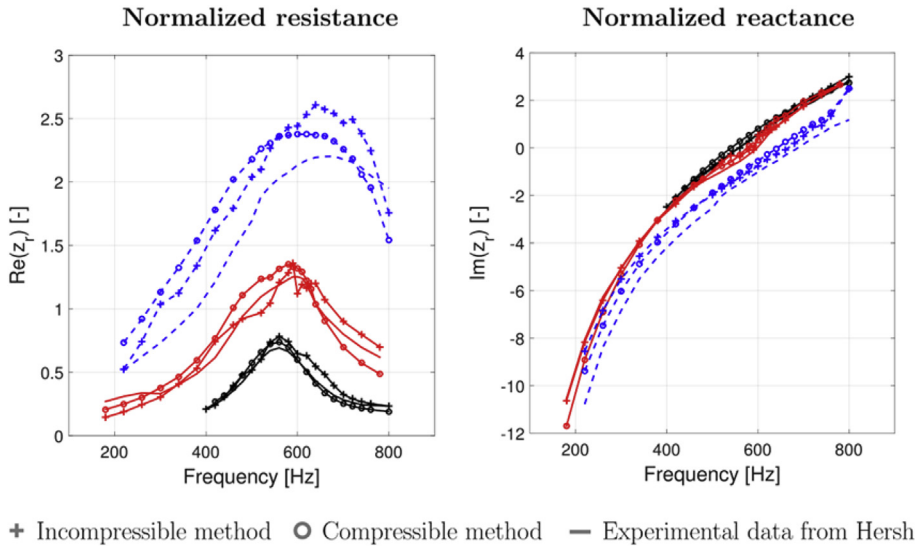

Fig. 58. Normalized resistance and reactance of a Helmholtz resonator at three SPLs - at 120 dB (black), 130 dB (red), and 140 dB (blue) - obtained from different approaches. (For interpretation of the references to colour in this figure legend, the reader is referred to the Web version of this article.)

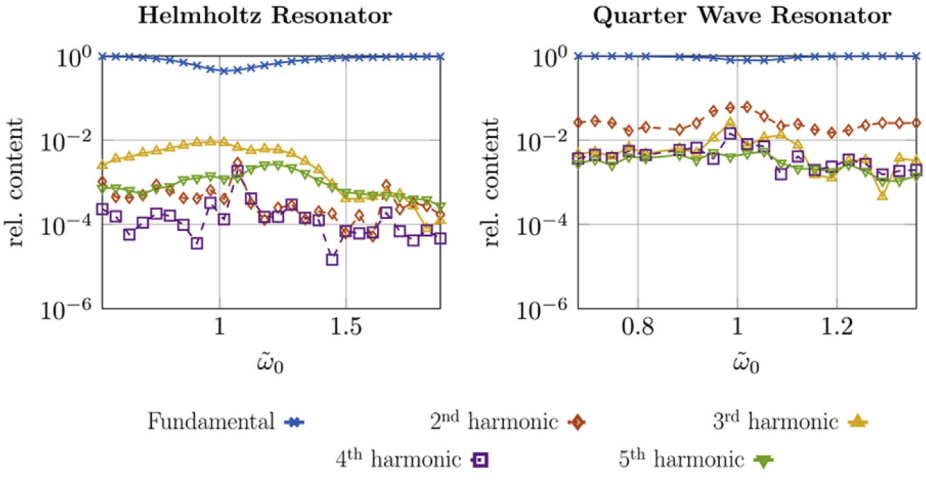

Fig. 59. Scattering to harmonics plotted in logarithmic scale for the case of a Helmholtz resonator with dominant odd harmonics (left) and of a quarter wave resonator without pattern in the harmonics (right), close to their eigenfrequency.

Please cite this article in press as: A.G. Wilson, Aeroacoustics research in Europe: The CEAS-ASC report on 2016 highlights, Journal of Sound and Vibration (2018), https://doi.org/10.1016/j.jsv.2017.10.016

constitutes a reasonable alternative to the more widespread one based on compressible solvers for the nonlinear acoustic characterization of Helmholtz resonators.

Additionally, energy scattering to higher harmonics has been investigated [60]. A commonly reported pattern in the spectrum of the orifice response, where the odd harmonics clearly dominate, is also captured numerically for Helmholtz resonators. It is analytically shown that this pattern is present due to the symmetry of the resonator neck. Accordingly, acoustic energy is also scattered to even harmonics if the geometrical symmetry is broken as for Helmholtz resonators with asymmetrical neck or quarter wave resonator. This work contributes to a global understanding of the nonlinear regime by linking local flow fields, global impedance, and the response spectrum. Sample results are shown in Figs. 58–60.

Submitted by J. Tournadre (jonathan.tournadre@kuleuven.be), W. De Roeck and W. Desmet, KU Leuven, Belgium, K. Förner and W. Polifke, Technische Universität München, Germany.

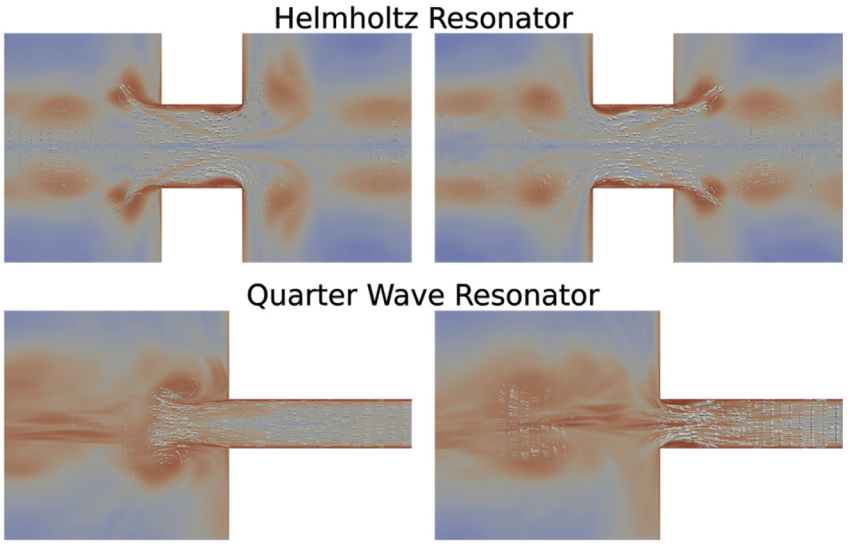

Fig. 60. Local flow field in the vicinity of the neck for both Helmholtz (top) and quarter wave (bottom) resonators: outflow conditions (left) and inflow conditions (right).

5. Further Applications of aeroacoustics

5.1. Combustion noise of premixed flames

The acoustic source mechanisms of turbulent slot flames (figs. 61–64) were investigated numerically using a hybrid LES/CAA approach. The acoustic flame response to the spatially integrated heat release fluctuations of the investigated rectangular

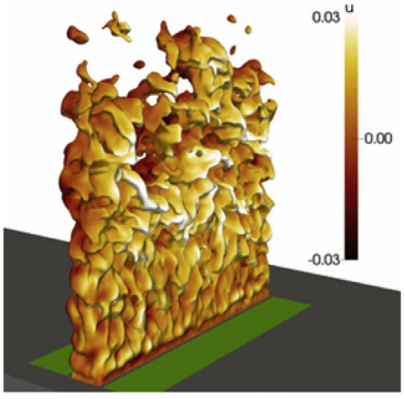

Fig. 61. Instantaneous flame surface of the investigated burner setup.

Please cite this article in press as: A.G. Wilson, Aeroacoustics research in Europe: The CEAS-ASC report on 2016 highlights, Journal of Sound and Vibration (2018), https://doi.org/10.1016/j.jsv.2017.10.016

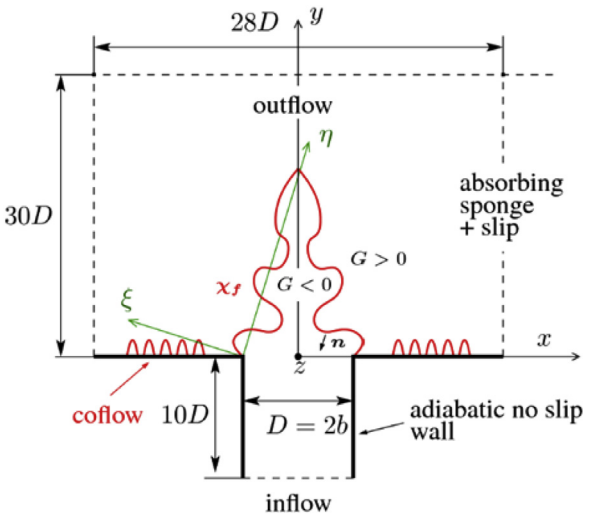

Fig. 62. Schematic of the investigated burner setup.

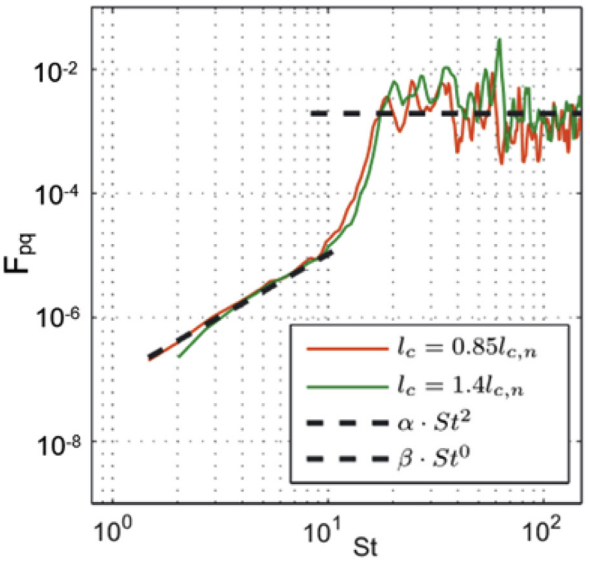

Fig. 63. Transfer function F_pq.

slot flames is similar to that of round flames [61], i.e., the transfer function $F_{pq} = [p'/\overline{p}]^2/[q'/\overline{q}]^2$ (St) shows a low frequency trend of αSt^2 for flame Strouhal numbers St < 20 and a plateau region βSt^0 for St ≳ 20 (Fig. 63) [62]. A spectral study of the local flame front deflection revealed that the low frequency acoustic emission is generated by the local heat release fluctuations due to the local flame front deflection.

The acoustic source distribution was analyzed with respect to hydrodynamic instability and shear layer effects. At low gas expansion ratios, the shear layer effect results in a strong vortex-flame interaction, i.e., the flame is strongly perturbed by the shear layer vortices leading to high flame front amplitudes at the flame base. At higher gas expansion ratios, the gas expansion effect significantly dampens the vortex-flame interaction at the flame base. However, due to the increased hydrodynamic instability effect, large flame front amplitudes and pockets are generated at the flame tip. The spatial analysis of the acoustic sources agreed with these findings [63,64]. That is, at low gas expansion ratios, the highest mean fluctuations of the acoustic energy source term are located at the flame base, whereas at high gas expansion ratios, the acoustic sound is mostly generated at the flame tip [62].

Submitted by S. Schlimpert, K. Pausch (k.pausch@aia.rwth-aachen.de)*, S. R. Koh, M. Meinke, W. Schröder, Institute of Aerodynamics, RWTH Aachen University, Wüllnerstr. 5a, D-52062 Aachen, Germany.*

Please cite this article in press as: A.G. Wilson, Aeroacoustics research in Europe: The CEAS-ASC report on 2016 highlights, Journal of Sound and Vibration (2018), https://doi.org/10.1016/j.jsv.2017.10.016

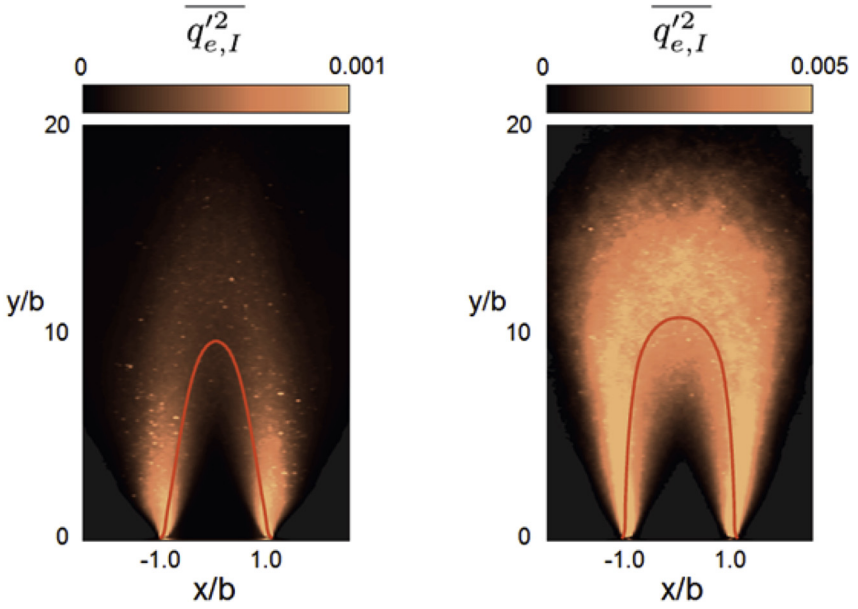

Fig. 64. Mean squared energy source at gas expansion ratio T_b/T_u = 2 (left) and T_b/T_u = 6.7 (right).

5.2. Tonal and silent wake modes of a square rod at incidence

The tonal sound produced by a rod with square cross section placed with its axis normal to a uniform subsonic flow has been measured [65]. The angle of incidence of the flow with respect to the basis of the cross section has been varied. The most interesting deviation between literature and the present experiments is the appearance of a silent wake mode. This silent mode appears by default when the wind tunnel is started for angles between 25 and 65°. It is metastable, an upstream perturbation, from small perturbations to hand waving, triggers the tonal wake mode. By perturbing the flow in wake of the rod, the silent mode can be recovered. The tonal mode appears spontaneously for angles between −25 and 25°. It is surprising that this behavior has not been reported before [65,66]. Numerical LES simulations, did not reproduce the silent mode [66].

Submitted by A. Hirschberg (A.Hirschberg@utwente.nl) and J.F. Dorneanu, UTwente, The Netherlands, A. Mueller, VKI, Belgium.

5.3. Acoustic multi-port characterization of modal filters containing micro-perforated panels

Within the IDEALVENT project, a set of modal filters with different lengths and panel properties has been studied numerically and experimentally at KU Leuven using the multi-port characterization framework [67]. This damper topology consists of a duct, where a micro-perforated panel (MPP) is installed at the velocity maxima of the first azimuthal duct modes [68]. This configuration therefore attenuates this specific azimuthal mode, leaving the other modes unaffected and resulting in only a minor aerodynamic pressure drop.

Experiments showed that the properties of the panel strongly influence the transmission coefficients of the element, while the reflection coefficients are nearly independent of the properties of the splitter plate. In terms of dissipated power, a higher panel resistance yields a higher acoustic power loss. The presence of a grazing flow over the MPP can significantly increase the attenuation of a modal filter, especially for panels with larger perforations. Such panels can therefore outperform panels with higher resistance, that yielded a higher power loss in quiescent conditions (Fig. 65).

The experimental work has been compared to numerical simulations using a Runge-Kutta discontinuous Galerkin discretization of the time-domain linearized Euler equations. The MPP is represented by a recursive time-domain transfer admittance formulation [69], using a rational approximation of the panel impedance. The multi-port characteristics of the modal filters have been computed from the simulation results using a time-domain characterization procedure [70]. The simulations predict the correct trends for all scatter matrix coefficients and a reasonable agreement of the amplitude is obtained (Fig. 66).

Submitted by H. Denayer (herve.denayer@kuleuven.be) *and W. Desmet, KU Leuven and Member of Flanders Make, Belgium, W. De Roeck, KU Leuven, Belgium.*

Please cite this article in press as: A.G. Wilson, Aeroacoustics research in Europe: The CEAS-ASC report on 2016 highlights, Journal of Sound and Vibration (2018), https://doi.org/10.1016/j.jsv.2017.10.016

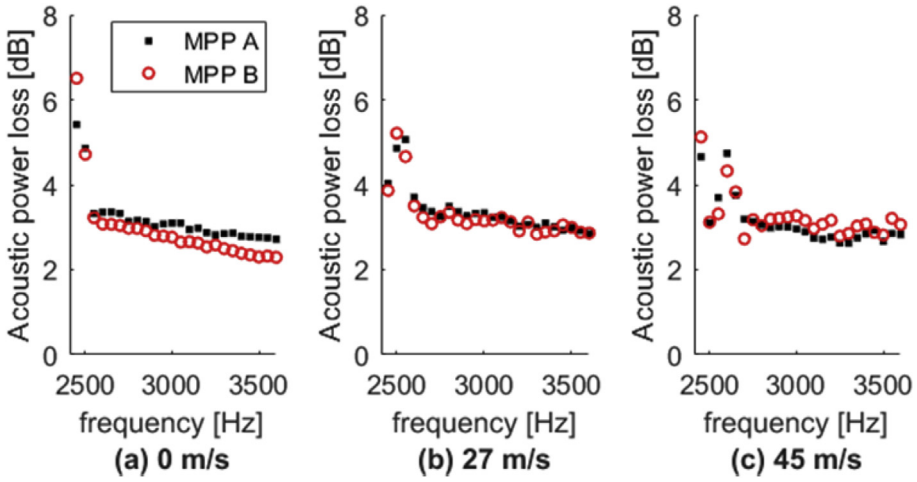

Fig. 65. Acoustic power loss of a modal filter with a diameter of D = 84 mm and a length of 4D, equipped with a standard micro-perforated panel (A) and a micro-perforated panel with larger perforations (B) for different flow velocities.

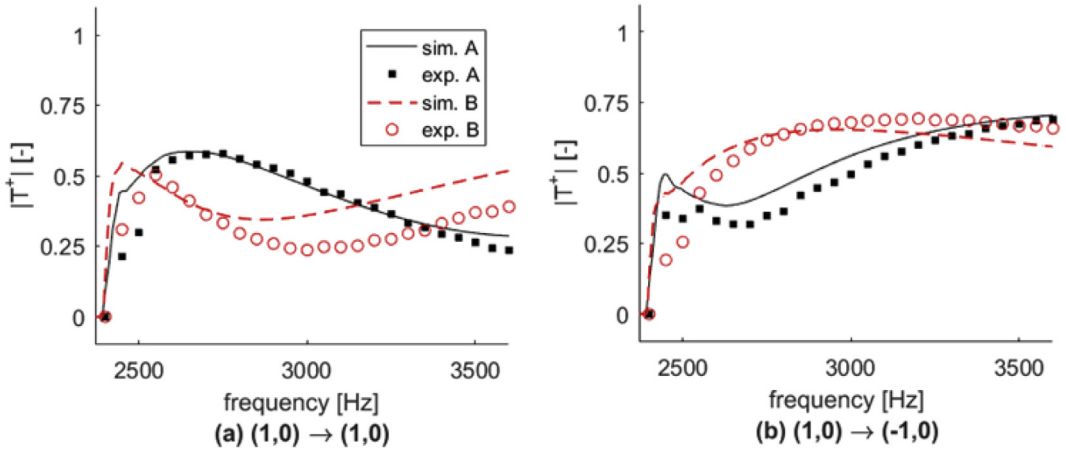

Fig. 66. Measured and simulated transmission coefficients of the (1,0)-mode to (a) itself and (b) the complex conjugate mode (−1,0) for a modal filter with a diameter of D = 84 mm and a length of 4D in a medium at rest.

References

[1] U. Kowarsch, C. Öhrle, M. Keßler, E. Krämer, Aeroacoustic simulation of a complete H145 helicopter in descent flight, J. Am. Helicopter Soc. 61 (4) (2016) 1–13.
[2] F. Boden, J.W. Delfs, Development of a Laser-based Sound Source, Honolulu, Inter-Noise, Hawaii, USA, 2006.
[3] K.-S. Rossignol, M. Lummer, J.W. Delfs, Validation of DLR's sound shielding prediction tool using a novel sound source, in: Proceedings of the 15th AIAA/CEAS Aeroacoustics Conference, Miami, USA, 2009.
[4] K.-S. Rossignol, J.W. Delfs, F. Boden, On the relevance of convection effects for a laser-generated sound source, in: Proceedings of the 21st AIAA/CEAS Aeroacoustics Conference, Dallas, USA, 2015.
[5] K.-S. Rossignol, J.W. Delfs, Analysis of the noise shielding characteristics of a NACA0012 2D wing, in: Proceedings of the 22nd AIAA/CEAS Aeroacoustics Conference, Lyon, France, 2016.
[6] T. Sinnige, D. Ragni, A.M.N. Malgoezar, G. Eitelberg, L.L.M. Veldhuis, APIAN-INF: an Aerodynamic and Aeroacoustic Investigation of Pylon-interaction Effects for Pusher Propellers, Manuscript submitted for publication, 2017.
[7] T. Sinnige, D. Ragni, G. Eitelberg, L.L.M. Veldhuis, Mitigation of pusher-propeller installation effects by pylon trailing-edge blowing, J. Aircraft 54 (1) (2017) 292–300. Helicopter Noise.
[8] N. Hu, Empirical spectral model of wall pressure fluctuations including adverse pressure gradient effects, in: 23rd AIAA/CEAS Aeroacoustics Conference, 2017.
[9] N. Hu, M. Herr, Characteristics of wall pressure fluctuations for a flat plate turbulent boundary layer with pressure gradients, in: 22nd AIAA/CEAS Aeroacoustics Conference, 2016.
[10] M.R. Catlett, J.M. Anderson, J.B. Forest, D.O. Stewart, Empirical modeling of pressure spectra in adverse pressure gradient turbulent boundary layers, AIAA J. 54 (2) (2016).
[11] A. Suryadi, M. Herr, Wall pressure spectra on a DU96-W-180 profile from low to pre-stall angles of attack, in: 21st AIAA/CEAS Aeroacoustics Conference, 2015.

Please cite this article in press as: A.G. Wilson, Aeroacoustics research in Europe: The CEAS-ASC report on 2016 highlights, Journal of Sound and Vibration (2018), https://doi.org/10.1016/j.jsv.2017.10.016

[12] R. Gojon, C. Bogey, O. Marsden, Investigation of tone generation in ideally expanded supersonic planar impinging jets using large-eddy simulation, J. Fluid Mech. 808 (2016) 90–115.
[13] R. Gojon, C. Bogey, Flow structure oscillations and tone production in underexpanded supersonic round impinging jets, AIAA J. 55 (2017) 1792–1805.
[14] C. Bogey, R. Gojon, Feedback loop and upwind-propagating waves in ideally-expanded supersonic impinging round jets, J. Fluid Mech. 823 (2017) 562–591.
[15] F.J. Zenger, H. Gert, S. Becker, S. Ennes, Sound source localization on an axial fan at different operating points, Exp. Fluid 57 (136) (2016) 1–10, https://doi.org/10.1007/s00348-016-2223-8.
[16] F. Zenger, H. Gert, S. Becker, Acoustic characterization of forward- and backward-skewed axial fans under increased inflow turbulence, in: Proceedings of 22nd AIAA/CEAS Aeroacoustics Conference, Lyon, France, 2016. AIAA Paper 2016-2943.
[17] F. Zenger, H. Gert, S. Becker, Acoustic characterization of forward- and backward-skewed axial fans under increased inflow turbulence, AIAA J. 55 (4) (2017) 1241–1250, https://doi.org/10.2514/1.J055383.
[18] F.J. Zenger, A. Renz, M. Becher, S. Becker, Experimental investigation of the noise emission of axial fans under distorted inflow conditions, J. Sound Vib. 383 (2016) 124–145, https://doi.org/10.1016/j.jsv.2016.07.
[19] C. Polacsek, V. Clair, T. Le Garrec, G. Reboul, M.C. Jacob, Numerical predictions of turbulence/cascade-interaction noise using computational aeroacoustics with a stochastic model, AIAA J. 53 (12) (2015) 3551–3566.
[20] G. Reboul, A. Cader, C. Polacsek, T. Le Garrec, R. Barrier, N. Ben Nasr, CAA prediction of rotor-stator interaction using synthetic turbulence: application to a low-noise serrated OGV, in: AIAA/CEAS Aeroacoustics Conference, 2017. Denver (USA).
[21] J. De Laborderie, S. Moreau, Analytical tonal fan noise prediction, J. Sound Vib. 372 (2016).
[22] S. Bouley, B. Francois, M. Roger, H. Posson, S. Moreau, On a two-dimensional mode-matching technique for sound generation and transmission in axial-flow outlet guide vanes, J. Sound Vib. 403 (2017).
[23] B. Francois, M. Roger, S. Moreau, Cascade trailing-edge noise modeling using a mode-matching technique and the edge-dipole theory, J. Sound Vib. 382 (2016).
[24] R. Hixon, Computational Aeroacoustics Prediction of Acoustic Transmission through a Realistic 2D Stator, 17th AIAA/CEAS Aeroacoustics Conference, Portland, OR, June 2011.
[25] M. Herr, R. Ewert, B. Faßmann, C. Rautmann, S. Martens, C.-H. Rohardt, A. Suryadi, Noise Reduction Technologies for Wind Turbines, NNFM, New Results in Numerical and Experimental Fluid Mechanics XI, Springer, DOI 10.1007/978-3-319-64519-3_55, 2018.
[26] R. Ewert, J. Dierke, J. Siebert, A. Neifeld, C. Appel, M. Siefert, O. Kornow, CAA broadband noise prediction for aeroacoustic design, J. Sound Vib. 330 (17) (2011) 4139–4160.
[27] C. Rautmann, Numerical Simulation of Wind Turbine Trailing-edge Noise, Dissertation, Technical University Braunschweig, Germany, 2017 (in print).
[28] A. Suryadi, S. Martens, M. Herr, Trailing-edge noise reduction Technologies for applications in wind energy, in: 23rd AIAA/CEAS Aeroacoustics Conference, 5–9 June 2017. Denver, CO, USA.
[29] M. Herr, K.-S. Rossignol, J.W. Delfs, M. Mößner, N. Lippitz, Specification of Porous Materials for Low-noise Applications, AIAA Paper 2014-3041, 2014.
[30] B.W. Faßmann, R. Ewert, J.W. Delfs, Prediction of Porous Trailing Edge Noise Reduction via Acoustic Perturbation Equations and Volume Averaging, AIAA Paper 2015-2525, 2015.
[31] L. Rossian, B.W. Faßmann, R. Ewert, J.W. Delfs, Prediction of Porous Trailing Edge Noise Reduction Using Acoustic Jump-conditions at Porous Interfaces, AIAA Paper 2016-2920, 2016.
[32] L. Rossian, R. Ewert, J.W. Delfs, Prediction of Porous Trailing Edge Noise Reduction by Application of Complex Porous Material, New Results in Numerical and Experimental Fluid Mechanics XI, Springer, 2017.
[33] C. Arce León, R. Merino-Martinez, D. Ragni, F. Avallone, M. Snellen, Boundary layer characterization and acoustic measurements of flow aligned trailing edge serrations, Exp. Fluid 57 (12) (2016) 182, https://doi.org/10.1007/s00348-016-2272-z.
[34] F. Avallone, S. Pröbsting, D. Ragni, Three-dimensional flow field over a trailing-edge serration and implications on broadband noise, Phys. Fluids 28 (11) (2016), https://doi.org/10.1063/1.4966633.
[35] F. Avallone, W.C.P. van der Velden, D. Ragni, Benefits of broadband serrations on broadband trailing-edge noise reduction, J. Sound Vib. 400 (2017) 167–177, https://doi.org/10.1016/j.jsv.2017.04.007.
[36] W.C.P. van der Velden, F. Avallone, D. Ragni, Numerical analysis of noise reduction mechanisms of serrated trailing edges under zero lift condition, in: 23rd AIAA/CEAS Aeroacoustics Conference, Denver, Colorado, USA, 5–9 June 2017.
[37] C. Colangeli, P. Chiariotti, K. Janssens, P. Castellini, A microphone clustering approach for improved generalized inverse beamforming formulation, in: INTER-NOISE and NOISE-CON Congress and Conference Proceedings (Vol. 251, No. 1, Pp. 770–780), Institute of Noise Control Engineering, 2015.
[38] C. Colangeli, P. Chiariotti, G. Battista, P. Castellini, K. Janssens, Clustering inverse beamforming for interior sound source localization application to a car cabin mock-up, in: The Proceedings of the Berlin Beamforming Conference, 2016.
[39] C. Colangeli, Clustering Inverse Beamforming and Multi-domain Acoustic Imaging Approaches for Vehicles NVH, Ph.D. thesis, Università Politecnica delle Marche, 2017.
[40] T. Bravo, C. Maury, Influence of source characteristics on the liner performance in a circular duct, in: Proceedings of the 14th AIAA/CEAS Aeroacoustics Conference, AIAA 2008-2976, Vancouver, British Columbia Canada, 5-7 May 2008.
[41] K. Strehl, Aplanatische und fehlerhafte Abbildung im Fernrohr, Zeitsch. Instrumen. 15 (1895) 362–370.
[42] L. Koop, K. Ehrenfried, Microphone-array processing for wind-tunnel measurements with strong background noise, in: 14th AIAA/CEAS Aeroacoustics Conference, 2008.
[43] J.R. Underbrink, Circularly symmetric, zero redundancy, planar array having broad frequency range application, US Patent No. 6,205,224, 2001.
[44] W.V. Bhat, Flight test measurement of exterior turbulent boundary layer pressure fluctuations on boeing model 737 airplane, J. Sound Vib. 14.4 (1971) 439–457.
[45] D. Palumbo, Deriving lifetime maps of coherent structures in the turbulent boundary layer, AIAA J. 46 (4) (2008) 810–823.
[46] D. Palumbo, Determining correlation and coherence lengths in turbulent boundary layer flight data, J. Sound Vib. 331 (16) (2012) 3721–3737.
[47] S. Haxter, C. Spehr, Comparison of model predictions for coherence length to in-flight measurements at cruise conditions, J. Sound Vib. 390 (2017) 86–117.
[48] A. Lyrintzis, Surface integral methods in computational aeroacoustics - from the (CFD) near-field to the (acoustic) far-field, Int. J. Aeroacoustics 2.2 (2003) 95–128.
[49] R. Ewert, W. Schröder, Acoustic perturbation equations based on flow decomposition via source filtering, J. Comput. Phys. 188.2 (2003) 365–398.
[50] M. Kaltenbacher, A. Hüppe, J. Grabinger, B. Wohlmuth, Modeling and finite element formulation for acoustic problems including rotating domains, AIAA J. 54 (12) (2016) 3768–3777.
[51] S. Sack, M. Åbom, K. Kucukcoskun, C. Schram, Generation and scattering of acoustic modes in ducts with flow, in: 20th AIAA/CEAS Aeroacoustics Conference, Atlanta, 2014.
[52] M. Shur, M. Strelets, A. Travin, J. Christophe, K. Kucukcoskun, C.F. Schram, S. Sack, M. Åbom, Effect of inlet distortions on ducted fan noise, in: 22nd AIAA/CEAS Aeroacoustics Conference, Lyon, 2016.
[53] A.M. Wohlbrandt, S. Guérin, R. Ewert, Extension of the Random Particle Mesh method to periodic turbulent flows for fan broadband noise prediction, in: 21st AIAA/CEAS Aeroacoustics Conference, Dallas, 2015.
[54] M. Roger, B. François, S. Moreau, Cascade trailing-edge noise modeling using a mode-matching technique and the edge-dipole theory, J. Sound Vib. 382 (2016) 310–327.
[55] M.J. Lighthill, On sound generated aerodynamically. I: general theory, Proc. R. Soc. 211 (1952) 564–587.

Please cite this article in press as: A.G. Wilson, Aeroacoustics research in Europe: The CEAS-ASC report on 2016 highlights, Journal of Sound and Vibration (2018), https://doi.org/10.1016/j.jsv.2017.10.016

[56] S.W. Rienstra, Acoustical detection of obstructions in a pipe with a temperature gradient, in: A. v. d Burgh (Ed.), Topics in Engineering Mathematics, Springer, Netherlands, 1992, pp. 151–179.
[57] K. Förner, A. Cárdenas Miranda, W. Polifke, Mapping the influence of acoustic resonators on rocket engine combustion stability, J. Propul. Power 31 (4) (Apr. 2015) 1159–1166.
[58] K. Förner, W. Polifke, Aero-acoustic characterization of Helmholtz resonators in the linear regime with system identification, in: 22nd International Congress on Sound and Vibration, Florence, Italy, 2015.
[59] J. Tournadre, K. Förner, W. Polifke, P. Martínez-Lera, W. Desmet, Determination of acoustic impedance for Helmholtz resonators through incompressible unsteady flow simulations, AIAA J. 55 (3) (2017) 790–798.
[60] K. Förner, J. Tournadre, P. Martínez-Lera, W. Polifke, Scattering to higher harmonics for quarter wave and Helmholtz resonators, AIAA J. 55 (4) (2017) 1194–1204.
[61] R. Rajaram, T. Lieuwen, Acoustic radiation from turbulent premixed flames, J. Fluid Mech. 637 (2009) 357–385.
[62] S. Schlimpert, S.R. Koh, K. Pausch, M. Meinke, W. Schröder, Analysis of combustion noise of a turbulent premixed slot jet flame, Combust. Flame 175 (2017) 292–306.
[63] S. Schlimpert, A. Feldhusen, J.H. Grimmen, B. Roidl, M. Meinke, W. Schröder, Hydrodynamic instability and shear layer effects in turbulent premixed combustion, Phys. Fluids 28 (1) (2016) 017104.
[64] S. Schlimpert, M. Meinke, W. Schröder, Nonlinear analysis of an acoustically excited laminar premixed flame, Combust. Flame 163 (2016) 345–367.
[65] J.F. Dorneanu, A. Mueller, P. Rambaud, E.T.A. v.d. Weide, A. Hirschberg, Tonal and silent wake modes of a square rod at incidence, Acta Acustica united Acustica 102 (2016) 419–422.
[66] A. Mueller, Large Eddy Simulation of Cross-flow Around a Square Rod at Incidence with Application to Tonal Noise Prediction, Dissertation, University of Twente (NL)/Von Kàrmàn Institute for Fluid Dynamics (Be), 2011.
[67] H. Denayer, V. Korchagin, W. De Roeck, W. Desmet, Multi-port characterization of a modal filter containing micro-perforated panels, in: Proceedings of the 22nd AIAA/CEAS Aeroacoustics Conference. Lyon, France, 30 May - 1 June 2016, 2016. AIAA 2016-2850.
[68] M. Abom, S. Allam, On the use of micro-perforates for Machinery and vehicle noise control, J. Acoust. Soc. Am. 132 (2012) 1887.
[69] H. Denayer, W. De Roeck, W. Desmet, A recursive transfer admittance formulation in time-domain, Submitted to J. Sound Vib. (2017).
[70] H. Denayer, V. Korchagin, R.M. Orselli, W. De Roeck, W. Desmet, Acoustic multi-port characterization of flow duct systems based on time-domain simulations, Submitted to J. Sound Vib. (2017).

Please cite this article in press as: A.G. Wilson, Aeroacoustics research in Europe: The CEAS-ASC report on 2016 highlights, Journal of Sound and Vibration (2018), https://doi.org/10.1016/j.jsv.2017.10.016